© 2019. Published by The Company of Biologists Ltd | Development (2019) 146, dev171652. doi:10.1242/dev.171652

HUMAN DEVELOPMENT

TECHNIQUES AND RESOURCES ARTICLE

Glycogen synthase kinase 3 induces multilineage maturation of human pluripotent stem cell-derived lung progenitors in 3D culture

Ana Luisa Rodrigues Toste de Carvalho[1,2,3,4], Alexandros Strikoudis[1,2], Hsiao-Yun Liu[1,2], Ya-Wen Chen[1,2], Tiago J. Dantas[5], Richard B. Vallee[5], Jorge Correia-Pinto[3,4] and Hans-Willem Snoeck[1,2,6,7,*]

ABSTRACT

Although strategies for directed differentiation of human pluripotent stem cells (hPSCs) into lung and airway have been established, terminal maturation of the cells remains a vexing problem. We show here that in collagen I 3D cultures in the absence of glycogen synthase kinase 3 (GSK3) inhibition, hPSC-derived lung progenitors (LPs) undergo multilineage maturation into proximal cells, type I alveolar epithelial cells and morphologically mature type II cells. Enhanced cell cycling, one of the signaling outputs of GSK3 inhibition, plays a role in the maturation-inhibiting effect of GSK3 inhibition. Using this model, we show NOTCH signaling induced a distal cell fate at the expense of a proximal and ciliated cell fate, whereas WNT signaling promoted a proximal club cell fate, thus implicating both signaling pathways in proximodistal specification in human lung development. These findings establish an approach to achieve multilineage maturation of lung and airway cells from hPSCs, demonstrate a pivotal role of GSK3 in the maturation of lung progenitors and provide novel insight into proximodistal specification during human lung development.

KEY WORDS: Directed differentiation, Human lung development, Pluripotent stem cells, Glycogen synthase kinase 3

INTRODUCTION

The generation of lung and airway epithelial cells from human embryonic stem (ES) and induced pluripotent stem (iPS) cells, collectively termed human pluripotent stem cells (hPSCs), holds major promise for studies in cellular physiology, disease modeling and regenerative medicine. Directed differentiation attempts to recapitulate development. The respiratory system originates from buds on the ventral anterior foregut endoderm (AFE) that undergo branching morphogenesis, culminating in the emergence of basal, goblet, club, ciliated and neuroendocrine cells in the stalks, which will become airways, while the distal tips widen into primitive alveoli (Swarr and Morrisey, 2015). Mature alveoli contain alveolar epithelial type I (ATI) cells, which are essential for gas exchange, and type II (ATII) cells, which produce surfactant [which is crucial for the maintenance of alveolar integrity by reducing surface tension (Whitsett et al., 2010)]. Thus, in order to generate lung and airway epithelial cells from definitive endoderm (DE) in hPSCs, anterior foregut endoderm (AFE), ventral AFE and lung progenitors (LPs) are sequentially specified followed by further differentiation into a mixture of alveolar and airway cells (Chen et al., 2017; Dye et al., 2016, 2015; Firth et al., 2014; Gotoh et al., 2014; Huang et al., 2015; Huang et al., 2014; Jacob et al., 2017; Konishi et al., 2016; McCauley et al., 2017; Mou et al., 2012; Wong et al., 2012).

Several challenges remain, however. Similar to other organs and tissues (Lancaster and Knoblich, 2014), terminal maturation remains elusive. We reported a 3D model consisting of lung bud organoids generated in suspension from early AFE followed by embedding in Matrigel, where branching morphogenesis with predominant generation of ATII cells ensued (Chen et al., 2017). These organoids were equivalent to the second trimester of human gestation. In other published models, maturation stage has not been reported or is also equivalent to early fetal lung (Table S1) (Dye et al., 2016, 2015; Firth et al., 2014; Gotoh et al., 2014; Huang et al., 2014; Jacob et al., 2017; Konishi et al., 2016; McCauley et al., 2017; Wong et al., 2012; Yamamoto et al., 2017). A method permissive for all mature lung epithelial cells would be useful to study lineage relationships, the mechanisms driving the specification of individual lineages, and the biology of mature human lung and airway cells, e.g. to investigate tropism of human respiratory viruses for specific cell types. A second challenge is that, although mouse genetic models have provided detailed insight into the initial stages of lung development (Chen et al., 2010; Domyan et al., 2011; Goss et al., 2009; Li et al., 2008; Malpel et al., 2000; Que et al., 2007; Weaver et al., 2000), the mechanisms underlying proximodistal specification, a prerequisite for generating more homogeneous populations of specific epithelial cells, are unclear. Canonical Wnt signaling, for example, is required for lung field specification (Goss et al., 2009; Zhang et al., 2008) and for the maintenance of distal tip progenitors (Ostrin et al., 2018) in the mouse, and has been reported to inhibit branching (Dean et al., 2005). In other genetic mouse models, however, Wnt signaling promoted distal differentiation (Mucenski et al., 2005, 2003; Shu et al., 2005). Notch signaling, on the other hand, plays a role in the differentiation of basal cells (BCs) and promotes a secretory fate (Mori et al., 2015; Rock et al., 2011; Tsao et al., 2008, 2009) while also inhibiting distal development in some mouse models (Tsao et al., 2008), but having the opposite (Dang et al., 2003; Guseh et al., 2009) or no effect (Xu et al., 2010) on distal development in others. The interpretation of these studies is complicated by the redundancy among ligands, receptors and downstream targets, potential leakiness and lack of faithfulness of reporters and Cre drivers, and the pharmacokinetics of inducing agents (e.g. doxycycline or tamoxifen). A well-defined *in vitro* hPSC-based model offers a complementary and more malleable

[1]Columbia Center for Human Development, Columbia University Medical Center, New York, NY 10032, USA. [2]Department of Medicine, Columbia University Medical Center, New York, NY 10032, USA. [3]Life and Health Sciences Research Institute (ICVS), School of Medicine, University of Minho, 4710-057 Braga, Portugal. [4]ICVS/3B's, PT Government Associate Laboratory, 4710-057 Braga/Guimarães, Portugal. [5]Department of Pathology and Cell Biology, Columbia University Medical Center, New York, NY 10032, USA. [6]Columbia Center for Translational Immunology, Columbia University Medical Center, New York, NY 10032, USA. [7]Department of Microbiology and Immunology, Columbia University Medical Center, New York, NY 10032, USA.

*Author for correspondence (hs2680@columbia.edu)

H.-W.S., 0000-0001-8375-995X

Received 6 September 2018; Accepted 13 December 2018

Development (2019) 146, dev171652. doi:10.1242/dev.171652

system where timing of addition and withdrawal of stimuli can be performed more precisely, and is directly relevant to human development.

It was recently reported that canonical Wnt signaling induced by the GSK3 inhibitor CHIR9902 (CHIR) promoted specification of developmental lung progenitors (LPs) towards ATII cells, whereas its withdrawal induced a proximal fate. These studies used reporter lines to enrich for progenitor populations or identify desired differentiated lineages (Jacob et al., 2017; Longmire et al., 2012; McCauley et al., 2017), and are therefore not universally applicable. Several other reports also show the generation of ATII cells (Chen et al., 2017; Huang et al., 2014; Jacob et al., 2017; Yamamoto et al., 2017). However, neither mature NGFR$^+$ basal cells (BCs) (Rock et al., 2009), the stem cells of the airways, nor ATI cells were ever generated, perhaps because both cell types arise late in development (Frank et al., 2016; Yang et al., 2018).

To address these issues, a culture model that does not rely on reporter lines and is permissive for the specification of all lung and airway lineages, thus allowing investigation of conditions that favor specific lineages, is required. Here, we report a collagen I (Col I) 3D culture system that satisfies these criteria. We show that GSK3 inhibition, rather than favoring distal fates as reported previously (McCauley et al., 2017), promotes proliferation and inhibits differentiation, whereas withdrawal of GSK3 inhibition induces multilineage proximal and distal maturation, including of NGFR$^+$ basal cells, morphologically mature ATII cells and cells with the morphology and marker expression of ATI cells. Furthermore, a WNT ligand could not recapitulate the effect of GSK3 inhibition, suggesting that this effect is not primarily mediated by canonical WNT signaling. Generic cell cycle inhibition, on the other hand, partially recapitulated the effect of CHIR withdrawal, suggesting a role for GSK3-mediated cell cycle regulation in maturation of LPs. We next used this model to show that, after CHIR withdrawal, NOTCH inhibition promotes proximal and inhibits distal development, thus identifying NOTCH signaling as one of the signaling pathways involved in proximodistal specification.

RESULTS

Establishment of a 3D Col I model of human lung and airway lineage specification

Our published 2D culture protocol recapitulates development (Huang et al., 2015, 2014). However, for further studies, the 2D model posed two problems. First, in large areas cell detachment occurred (Huang et al., 2015). Second, despite ample presence of cells expressing ATII markers, expression of the most specific ATII marker, SFTPC, was sporadic whereas ATI cells and BC-like cells were rare (Huang et al., 2015, 2014), and mature NGFR$^+$ BCs were absent. We therefore proceeded to culture in a 3D matrix.

We generated NKX2.1$^+$FOXA2$^+$ LPs, which lacked mature lung and mesenchymal markers, in 2D until day (d)25, when the purity of NKX2.1$^+$FOXA2$^+$ lung progenitors was maximal (90-98%), as described previously (Huang et al., 2015, 2014), and transferred these to Col I gels in the presence of factors used in 2D cultures (Huang et al., 2015, 2014) [CHIR, FGF10, KGF and dexamethasone, 8-bromo-cAMP and isobutylmethylxanthine (DCI) (Gonzales et al., 2002)] (Fig. 1A, top). The cells organized in strands enveloping empty lacunae (Fig. 1A, upper left) and almost uniformly expressed NKX2.1 (85.08±17.54%) (Fig. 1A), FOXA2 (not shown) and the surface mucin MUC1, the apical expression of which indicated polarization (Fig. 1A). Most cells also co-expressed variable amounts of SOX9 and SOX2 (Fig. 1A), which, in contrast to the mouse (Rockich et al., 2013), are commonly co-expressed in distal tips during human lung development (Chen et al., 2017; Nikolic et al., 2017). SFTPC$^+$ cells were abundant, indicating that a 3D environment is crucial for SFTPC expression (Fig. 1A). The ATII marker ABCA3 was also detected (Fig. 1A). Some cells co-expressed ATI (PDPN) and ATII (SFTPB, SFTPC) markers (Fig. 1A, arrows) (Desai et al., 2014; Treutlein et al., 2014). Cells expressing markers of both ATI and ATII cells, called bipotential progenitors, are found at the distal tips of the developing lung in mice and may differentiate into ATI or ATII cells (Desai et al., 2014; Treutlein et al., 2014), although more recent evidence suggests that the ATI-ATII fate decision is made earlier in development (Frank et al., 2016; Zacharias et al., 2018). We also observed cells co-expressing PDPN, SFTPC and NKX2.1 in the bud tips of W14 human fetal lung (Fig. S2A). Other ATI (CAV1, AKAP5, CLIC5, SCNN1A, COL4, AQP5) (Treutlein et al., 2014) and proximal (CC10, MUC5B, P63) markers were not observed (Fig. S1), and neither were mesodermal (PDGFRα, CD90) and endothelial markers (CD31) (not shown).

Removing the GSK3 inhibitor at the initiation of the 3D cultures at d25 (CHIR−) (Fig. 1B, top) dramatically changed morphology and marker expression. Comparative immunofluorescence for 18 markers is shown in Fig. S1. The cells were arranged in more discrete colonies, expressed the endodermal marker FOXA1, but mostly lost NKX2.1 (Fig. S2B) which, later in lung development, is restricted to ATII and airway club cells. Markers for ATI cells, HOPX (Fig. S2B), PDPN and ATI markers distilled from the RNAseq data of Treutlein et al. (2014) (COL4, CAV1, CLIC5 and AKAP5) were widely expressed (Fig. 1B, Fig. S1) in flattened cells (Fig. 1B, Figs S1, S2B), some of which stained for SCNN1A, which is also expressed in ATI cells (Fig. 1B, Fig. S1) (Yang et al., 2016). COL4 was expressed basally (Fig. 1B, Fig. S1), consistent with alveolar basement membrane production by ATI cells. These changes in morphology and combined marker expression indicate ATI specification. Other markers of mature ATI cells, such as AGER, were not detected, suggesting still incomplete maturation. In addition, multiple clusters of P63$^+$ (Fig. 1B, Figs S1, S2B) and KRT5$^+$ cells (Figs S1, S2B), a phenotype compatible with airway basal cells (BCs) (Rock et al., 2009), and cells expressing markers of differentiated airway cells [AcTUB$^+$ (ciliated), CC10$^+$ (club) and MUC5B$^+$ (goblet)] were observed (Fig. 1B, Fig. S1). Closer examination further revealed that these markers occurred in epithelial structures that appeared polarized, with KRT5$^+$ and P63$^+$ cells on the basal side, and AcTUB on the apical side (Fig. 1B, Fig. S2C). These expression patterns suggest that Col I culture of LPs in the absence of CHIR induced multilineage, proximal and distal differentiation. Light sheet microscopy (Fig. 2A) showed irregularly shaped structures with markers for airway cells (MUC5B, AcTUB, CC10, CGRP) occurring in discrete peripheral clusters, the BC marker KRT5 lining the outside of the structures, and the distal markers HT2-280 (ATII cells) and CAV1 (ATI cells) expressed more diffusely. Although Col I cultures do not generate structurally appropriate lung organoids, these qualitative findings confirm that CHIR withdrawal induces multilineage differentiation and maturation.

Electron microscopy indicates enhanced multilineage maturation in CHIR− cultures

Transmission electron microscopy (TEM) of CHIR+ cultures showed mostly cuboidal cells (Fig. 2Bi) with apical cytoplasmic projections (Fig. S2D), suggestive of polarization. Many contained lamellar bodies (LBs) at various stages of maturation, although most appeared as multivesicular bodies, the precursors of LBs (Weaver

Development (2019) 146, dev171652. doi:10.1242/dev.171652

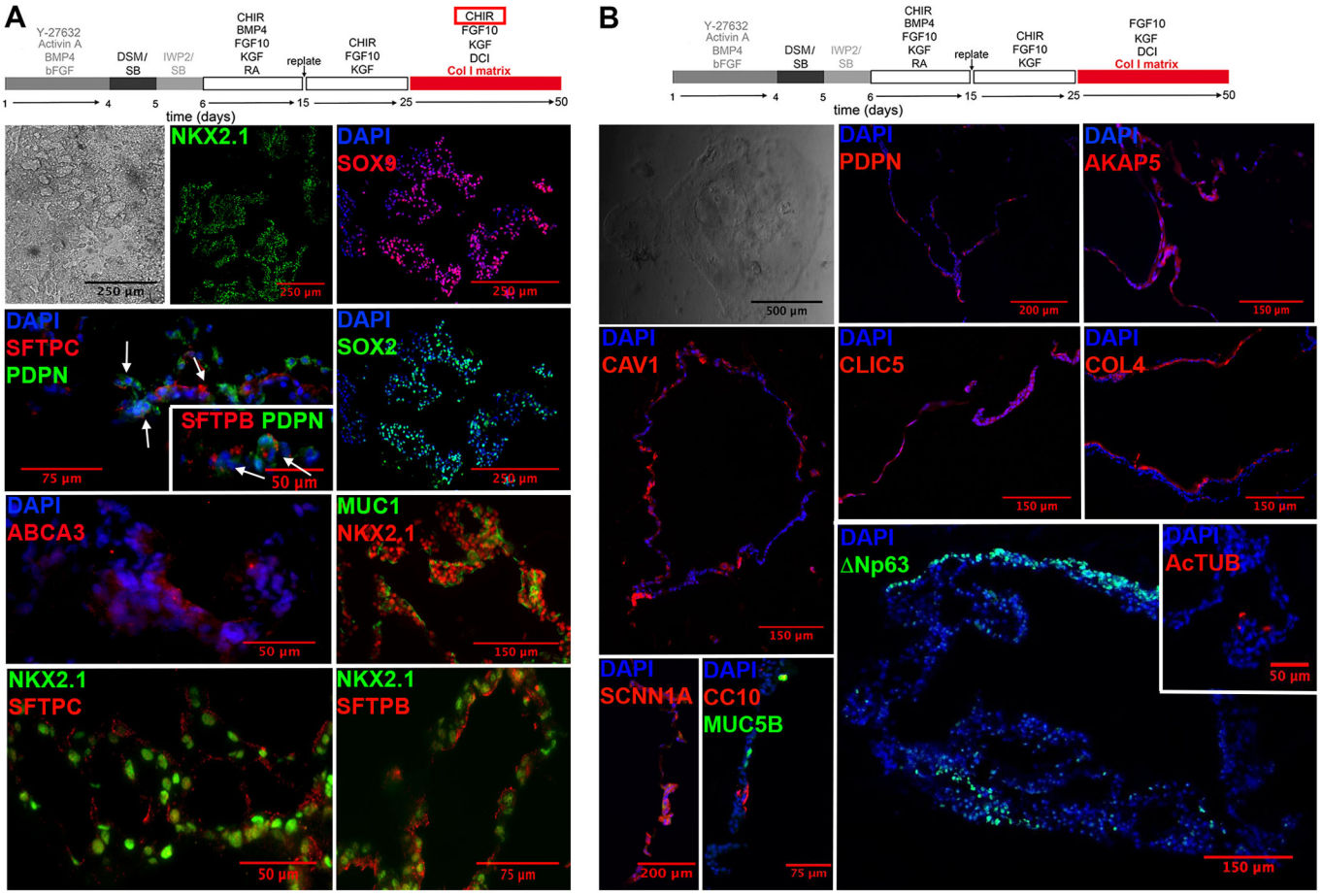

Fig. 1. CHIR withdrawal induces maturation. (A) Bright-field views and immunofluorescence of indicated markers after culture of RUES2 ESCs in the presence of CHIR, according to the protocol above (representative of over 12 experiments; arrows indicate cells co-expressing ATII and ATI markers). (B) Bright-field views and immunofluorescence of indicated markers after culture of RUES2 ESCs in the absence of CHIR according to the protocol above (representative of over 12 experiments).

et al., 2002) (Fig. 2Bi; Fig. S2D, arrows). In CHIR− conditions, cells with LBs were much sparser, consistent with reduced expression of ATII markers, but contained uniformly mature electron-dense LBs (Fig. 2Bii; Fig. S2E, arrows), indicating maturation. Elongated cells (Fig. 2Biii, Fig. S2F) lining a lumen that appeared free of matrix and with, in some instances, electron-dense material compatible with basement membrane (Fig. S2G, arrow), a morphology compatible with ATI cells, were present. We also observed club cells with secretory granules (Fig. 2Biv), as well as ciliated cells (Fig. 2Bv; Fig. S2H, arrow) reaching the lumen. Other luminal cells had indeterminate morphology and could be precursors of goblet or club cells. These morphological findings are consistent with the immunofluorescence data, and indicate that withdrawal of CHIR induced multilineage maturation.

Quantitative analysis of CHIR-treated and CHIR− Col I cultures

To further substantiate the induction of multilineage differentiation in the absence of CHIR, we quantified differentiation in the cultures. In CHIR− cultures, cell density was significantly lower than in CHIR+ cultures (Fig. 3A,B), $15±7×10^6$ versus $163±45×10^6$ cells/10^6 ESCs (n=4), indicating that CHIR supports proliferation of progenitors. mRNAs encoding markers for ATI, ciliated, club, neuroendocrine and basal cells were massively upregulated (10^2 to 10^6-fold) in CHIR− compared to CHIR+ cultures (Fig. 3C). Although transmission electron microscopy revealed that ATII cells in CHIR− cultures were morphologically mature, mRNAs for ATII markers were downregulated in CHIR− compared with CHIR+ conditions, most likely because cells expressing ATII markers are precursors for both mature ATII and ATI cells (Nabhan et al., 2018; Zacharias et al., 2018), and are the most abundant in the CHIR+ condition. These data therefore support the conclusion that CHIR withdrawal induced multilineage maturation. Quantification of immunofluorescence images confirmed a decreased fraction of $NKX2.1^+$ nuclei (24.16±18.59%) (Fig. 3D) and increased proportion of $P63^+$ nuclei (34.52±2.25%) (Fig. 3E). Furthermore, quantification of non-nuclear markers by measuring fluorescent area relative to DAPI-positive area showed an increase in all tested differentiation markers in CHIR− compared with CHIR+ cultures (Fig. 3F). Flow cytometry revealed an increase in the proportion of cells expressing HT2-280 (4.89±1.06% versus 0.75±0.28%) (Fig. 4A), a marker for more mature ATII cells, and a strikingly increased fraction and absolute number of $ITGA6^+ITGB4^+$ cells, which were undetectable in CHIR+ conditions, but reached 24±12% in CHIR− conditions (Fig. 4B). This phenotype is associated with airway progenitors (Rock et al., 2009). To further confirm the BC-like identity of these cells, we purified $ITGA6^+IGTB4^+$ cells using fluorescence-activated cell sorting and stained for BC markers. All cells co-expressed the BC markers p63, MUC1, KRT5, SOX2 and PDPN

Development (2019) 146, dev171652. doi:10.1242/dev.171652

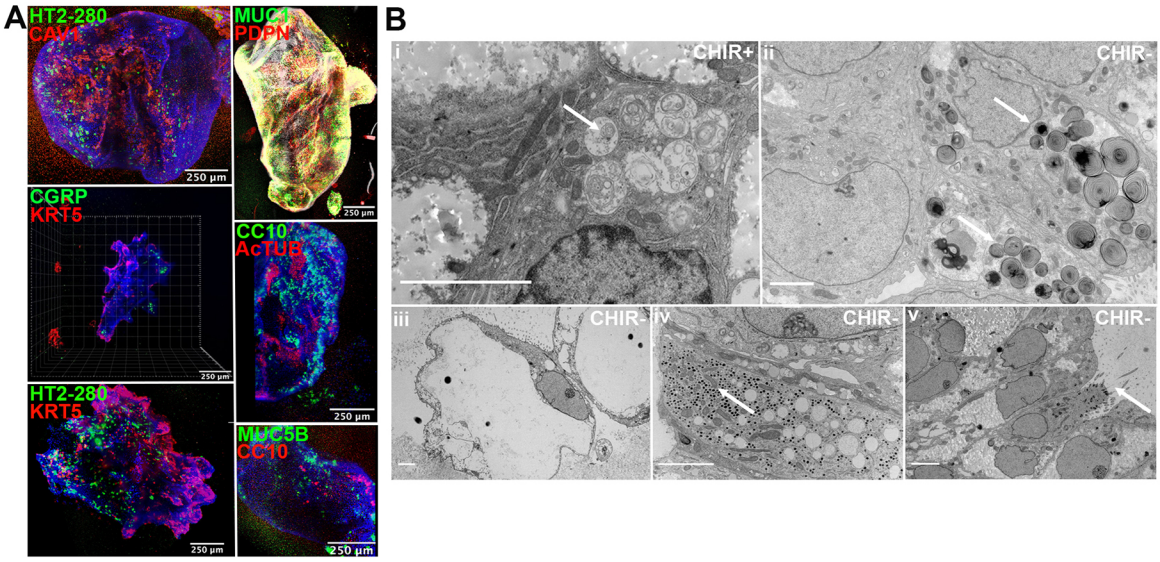

Fig. 2. Light sheet and transmission electron microscopy of CHIR− cultures. (A) Whole-mount immunofluorescence of the indicated differentiation markers in CHIR− cultures at d50 (representative of three independent experiments). (B) Transmission electron microscopy of CHIR+ and CHIR− cultures at d50. (i) Cell with immature LBs and multivesicular bodies (arrow) in CHIR+ conditions; (ii) cell with mature LBs (arrow) in CHIR− conditions; (iii) flat cells compatible with ATI cells in CHIR− conditions; (iv) club cell (arrow) in CHIR− conditions; (v) ciliated cell (arrow) in CHIR− conditions (all data from i-v are representative of n=1). Scale bars: 250 µm in A; 3 µm in B.

(Fig. 4C), indicating that these are indeed BC like. Furthermore, in human adult lung, ITGB4 was expressed specifically in the basal layer of airway epithelium, whereas ITGA6 was also sporadically expressed distally (Fig. 4D). Finally, after longer culture, the adult BC marker NGFR (Huang et al., 2014; Rock et al., 2009) was amply detected in epithelial structures in CHIR− conditions (Fig. 4E) with $EPCAM^+NGFR^+$ cells comprising 16.5±5.85% ($4.56±1.8×10^4$ cells cm^{-2}) of the total number of cells at d80 (Fig. 4F). We next isolated $EPCAM^+ITGB4^+NGFR^+$ cells, and expanded these on 3T3-J2 feeders in the presence of the ROCK inhibitor Y27632 (Butler et al., 2016). After two passages, during which the cells maintained their $ITGB4^+NGFR^+$ phenotype (Fig. 4G) and displayed a doubling time of ∼0.8 days (Fig. 4H), the cells were plated in air-liquid interphase cultures, where they differentiated into goblet, club and ciliated cells after 6 weeks (Fig. 4I). These observations demonstrate that mature $NGFR^+$ BCs were generated. Taken together, quantitative analysis of the cultures indicates induction of multilineage differentiation and maturation in the absence of CHIR.

Genome-wide expression analysis confirms multilineage maturation in CHIR− Col I cultures

Genome-wide expression analysis and cross-referencing with the single cell expression data of Treutlein et al. in fetal mouse lung (Treutlein et al., 2014) revealed that, although many transcripts associated with the ATII lineage were variably affected (Fig. 5A), most transcripts indicative of ATI, ciliated and club cell differentiation as well as BC markers and secreted mucins (Fig. 5B-F) were upregulated, confirming multilineage maturation in CHIR− cultures.

To assess maturity with respect to human development, we cross-referenced the RNAseq data with the KeyGenes database, which contains expression profiles of human organs during 1st and 2nd trimesters of gestation and adulthood (Roost et al., 2015). D25 LPs showed the best match with the first trimester lung, consistent with their early stage of development. Cells from CHIR-treated cultures corresponded to the 2nd trimester. Cells from CHIR− cultures corresponded to 1st and 2nd trimester and to adult lung (Fig. 5G), a finding most likely explained by the large diversity of cell types at varying stages of differentiation. The fact that only cells cultured in CHIR− conditions matched with human adult lung is consistent with further maturation in this condition.

Finally, single cell RNAseq and t-SNE analysis showed several clusters of cells in CHIR− conditions that could be assigned to specific cell types (airway progenitors, club cells, ATI cells and NE cells) based on key markers (Fig. S3). Using the same markers, none of these populations could be identified in CHIR+ conditions (Fig. S3). These data again demonstrate multilineage differentiation induced by CHIR removal.

Effect of varying culture conditions

We next compared Col I and Matrigel as 3D media. Although a differentiation-inducing effect was also noted in CHIR− conditions in Matrigel (Fig. S4A,B), expression of markers of mature cells was significantly lower than in Col I (Fig. S4C). Col I is therefore more permissive for multilineage maturation than Matrigel. It has also been suggested that replacing KGF by FGF2 and higher concentrations of FGF10 are more efficient for generating proximal cells (McCauley et al., 2017). However, except for SFTPC, expression of most markers was lower in this condition (Fig. S4D), although proximal and distal markers could be detected by immunofluorescence (Fig. S4E).

Finally, as CHIR is an agonist of canonical WNT signaling, which shows stage-specific effects during lung development (Swarr and Morrisey, 2015), we explored early (d15) and late (d35) CHIR withdrawal. Delayed withdrawal at d35 increased cell density (Fig. S5A), and even further increased the absolute number of both $ITGA6^+IGTB4^+$ BC-like cells ($5.42±1.6×10^4$ cells cm^{-2}) (Fig. S5B) and $HT2\text{-}280^+$ ATII cells ($4.59±3×10^4$ cells cm^{-2}) (Fig. S5C), as well as mRNA expression for most differentiation markers (Fig. S5D) compared with CHIR withdrawal at d25. Immunofluorescence confirmed the ample presence of differentiation markers when CHIR was withdrawn at d35 (Fig. S5E) and quantification showed increased expression of all markers at the protein level (Fig. S5F). This finding is consistent with additional CHIR-driven progenitor expansion followed by

Development (2019) 146, dev171652. doi:10.1242/dev.171652

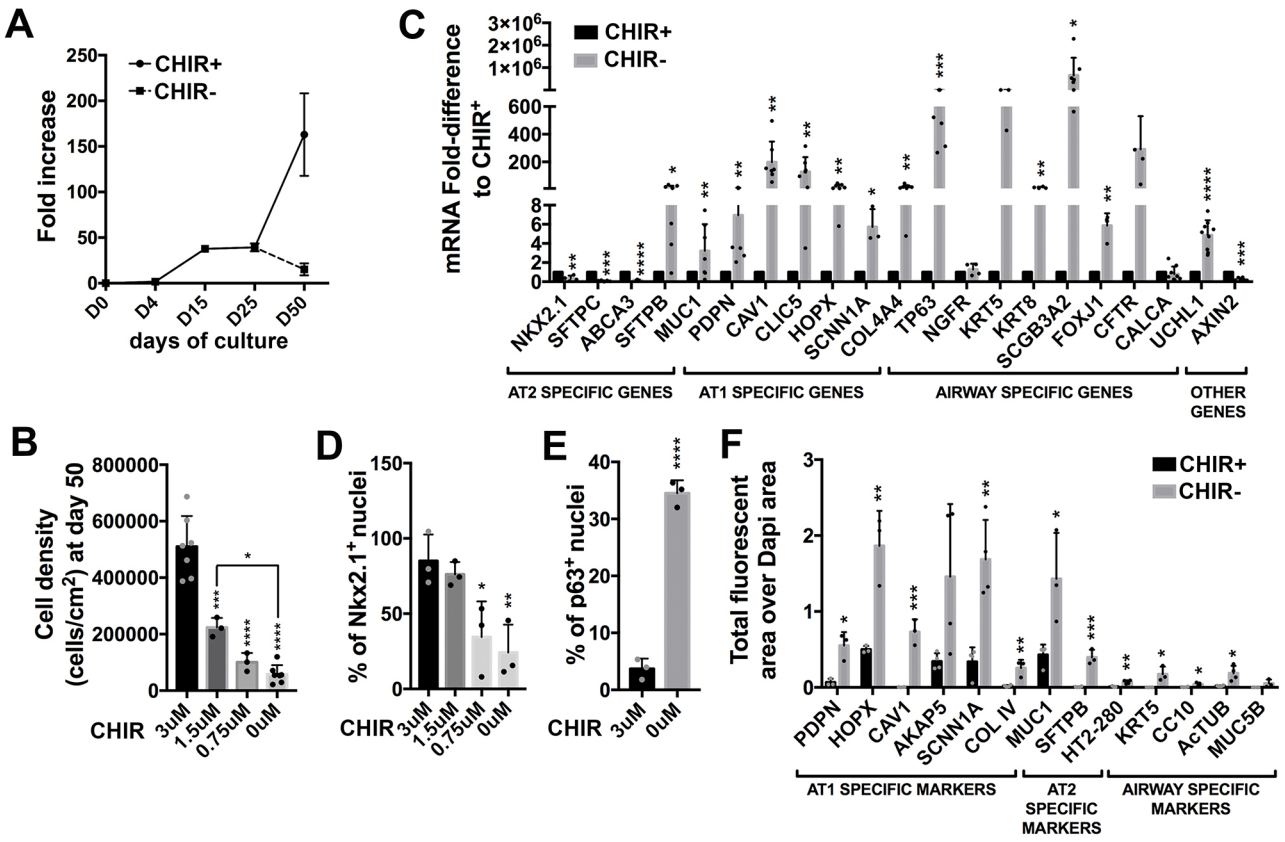

Fig. 3. Quantitative analysis of CHIR+ and CHIR− cultures. (A) Cellular expansion starting from undifferentiated RUES2 ESCs in CHIR+ and CHIR− cultures (data are mean±s.d., *n*=4 independent experiments). (B) Cellular expansion from d25 to d50 in the presence of varying concentrations of CHIR (data are mean±s.d.; 3 µM and 0 µM; *n*=7; 1.5 µM and 0.75 µM; *n*=3, **P*<0.05, ****P*<0.001, *****P*<0.0001). (C) Expression of mRNA for differentiation markers in CHIR− cultures relative to CHIR+ cultures (data are mean±s.d., *n*=3-7 independent experiments, **P*<0.05, ***P*<0.01, ****P*<0.001, *****P*<0.0001; see Table S4 for exact number of replicates per gene). (D) Fraction of NKX2.1$^+$ nuclei in d50 cultures after culture from d25 to d50 in varying concentrations of CHIR (data are mean±s.d., *n*=3, **P*<0.05, ***P*<0.01). (E) Fraction of P63$^+$ nuclei in d50 cultures after culture from d25 to d50 with or without CHIR (data are mean±s.d., *n*=3 independent experiments, *****P*<0.0001). (F) Relative quantification of immunofluorescence for non-nuclear protein, as determined by the ratio between fluorescent area for a given marker and nuclear DAPI area (data are mean±s.d., *n*=4 independent experiments, **P*<0.05, ***P*<0.01, ****P*<0.001).

multilineage differentiation after CHIR withdrawal. In contrast, early CHIR withdrawal at d15 severely compromised the competence of LPs to express differentiation markers (Fig. S5G). This finding is consistent with those of Ostrin et al. (2018), who also showed that competence to express lung markers is compromised after early withdrawal of CHIR from 2D cultures. Taken together, Col I is optimally permissive for multilineage differentiation, although timing of CHIR withdrawal is crucial to ensure the competence of LPs to undergo multilineage differentiation but it does not affect proximodistal specification.

The effect of CHIR is not reproduced by canonical WNT signaling

CHIR is frequently used as an agonist of canonical WNT signaling (Jacob et al., 2017; McCauley et al., 2017), as canonical WNT signaling inhibits GSK3 Ser/Thr kinase activity, thereby stabilizing β-catenin (Willert and Nusse, 2012). CHIR increased AXIN2 mRNA levels (Fig. 3C), nuclear β-catenin and inhibitory S9 phosphorylation of GSK3 (Fig. 6A), indicating GSK3 inhibition and WNT activation, as expected. We therefore assessed the specific effect of the canonical WNT ligand WNT3A in CHIR− conditions. WNT3A did not affect cellular expansion (Fig. 6B) and even further increased the fraction of ITGA6$^+$ITGB4$^+$ cells (31.8±12.95%) (Fig. 6C), the number of P63$^+$ nuclei (51.5±9.78%) (Fig. 6D) and KRT5 pixel number (Fig. 6E), while not affecting the fraction of HT2-280$^+$ ATII cells (not shown) (comparative immunofluorescence for 18 markers shown in Fig. S1). WNT3A did not increase TP63 or KRT5 mRNA, but increased mRNAs for club cell markers (NKX2.1, SFTPB and SCGB3A2) (Fig. 6F). WNT3A, which was biologically active, as determined by induction of the WNT target AXIN2 (Fig. 6F) and increased nuclear β-catenin (Fig. S4F), therefore neither qualitatively nor quantitatively recapitulated the effect of CHIR. Contrary to previous reports (Jacob et al., 2017; McCauley et al., 2017), our findings indicate that WNT signaling does not promote distal fate at the expense of proximal fate, but in fact has an opposite effect by modestly favoring a proximal and club cell fate. Because WNT3A neither quantitatively nor qualitatively replicated the effects of CHIR, it is unlikely that the differentiation-inhibiting effects of CHIR depend on WNT agonism.

The effect of cell cycle regulation by GSK3

GSK3 integrates inputs from multiple signaling pathways and one of its outputs is cell cycle regulation. Because in neural progenitors, cell cycle arrest induces differentiation (Calegari et al., 2005; Calegari and Huttner, 2003; Kim et al., 2009; Lange et al., 2009; Roccio et al., 2013), we tested the hypothesis that some of the effects of CHIR withdrawal might be due to a lengthening of the cell cycle, while GSK3 inhibition might prevent differentiation by enhancing cycling and in doing so prevent maturation. We added two cell cycle inhibitors that act through distinct mechanisms, a

Development (2019) 146, dev171652. doi:10.1242/dev.171652

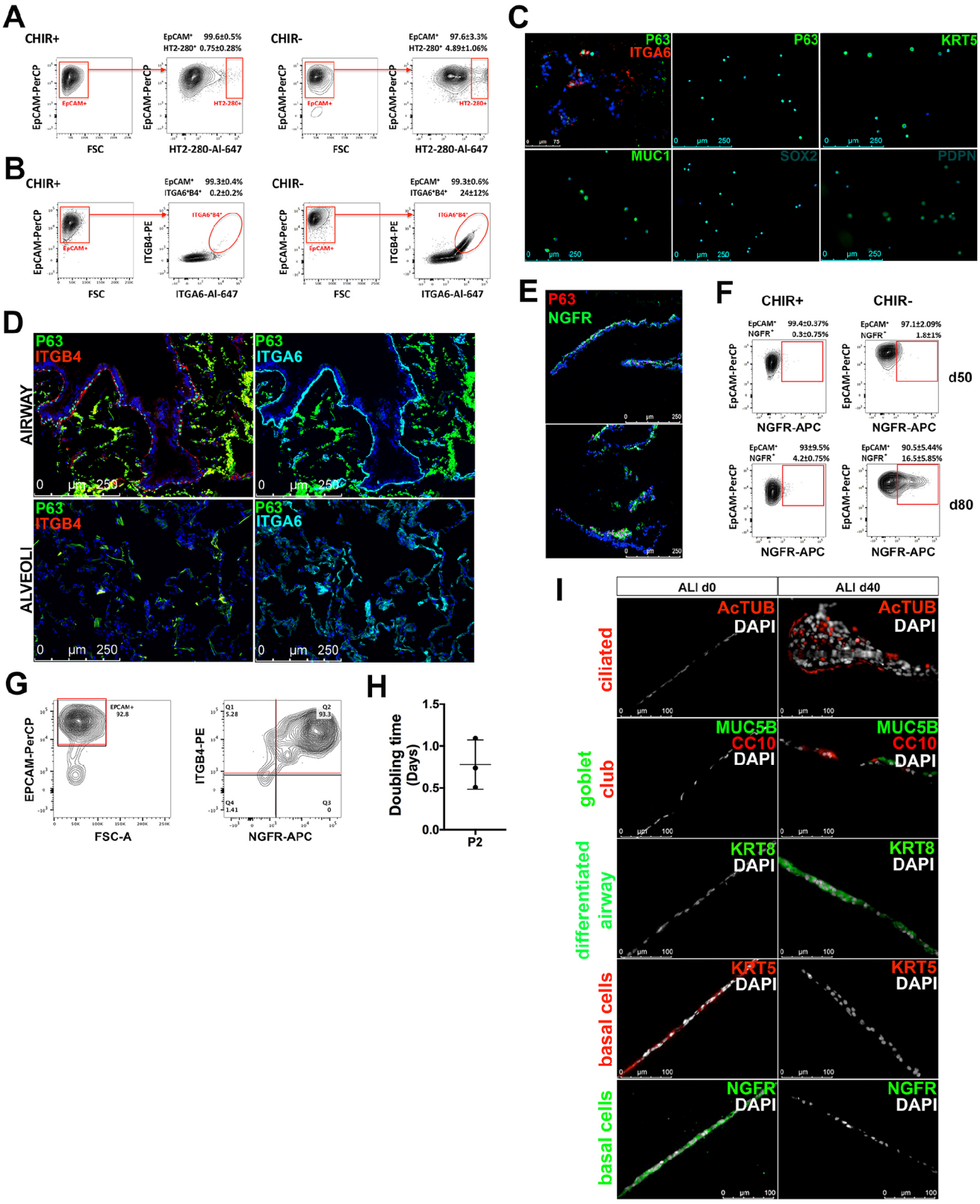

Fig. 4. See next page for legend.

CDK4/6-inhibitor (PD0332991, PD) (Dickson, 2014) and a CDC7 inhibitor (XL413, XL), to CHIR+ cultures. Although subtle differences were observed between both inhibitors, both PD and XL decreased cellularity (Fig. 7A,D), upregulated mRNAs for all differentiation markers, and strikingly increased expression of mRNAs for distal and ATII markers (Fig. 7B,E). Upregulation of proximal markers was more variable. p63 mRNA was increased more by XL than by PD. Induction of SCGB3A2 was highly

Development (2019) 146, dev171652. doi:10.1242/dev.171652

Fig. 4. Airway progenitors and distal cells in CHIR– cultures. (A) Representative example and statistical analysis of the flow cytometric profile after staining for EPCAM and HT2-280 of cells from CHIR+ and CHIR– cultures (*n*=4 independent experiments). (B) Representative example and statistical analysis of the flow cytometric profile after staining for EPCAM, ITGA6 and ITGB4 of cells from CHIR+ and CHIR– cultures (*n*=4 independent experiments). (C) Staining of CHIR– cultures for P63 and ITGA6 (upper left corner) and immunofluorescence for the indicated markers on preparations of ITGA6^{+}ITGB4^{+} cells isolated from CHIR– cultures by flow cytometric cell sorting (representative of one experiment). (D) Expression patterns of ITGB4, ITGA6 and P63 in human adult airway and alveoli by immunofluorescence staining (representative of one human adult lung sample). (E) Immunofluorescence staining for NGFR and P63 in cultures differentiated in CHIR– conditions until d120 (representative of *n*=3 independent experiments). (F) Representative example and statistical analysis of the flow cytometric profile after staining for EPCAM and NGFR of cells from CHIR+ and CHIR– cultures at d50 and d80 of the differentiation protocol (*n*=6 independent experiments). (G) Representative analysis of expression of EPCAM, ITGB4 and NGFR after two passages of purified NGFR^{+}ITGB4^{+} cells from d80 CHIR– cultures in the presence of 3T3-J2 cells and ROCK inhibitor (RI). (H) Doubling time of cells in G (data are mean±s.d.; *n*=3 independent experiments). (I) Immunofluorescence of cells in G at initiation and after 40 days of air-liquid interphase culture.

variable and not significant with XL, whereas PD appeared to repress the little SCGB3A2 expression there was in CHIR+ cultures. Immunofluorescence confirmed widespread induction of distal markers in CHIR+ cultures in the presence of PD or XL (Fig. 7C,F, comparative immunofluorescence for 18 markers shown in Fig. S6). Furthermore, in the presence of either PD or XL, the frequency of the ATII marker HT2-280, which was virtually absent in CHIR+ conditions, was similar to that observed in CHIR– conditions (Fig. 7G,H). On the other hand, although the fraction of P63^{+} nuclei was variably increased in both conditions (Fig. 7I), expression levels of ITGA6 and ITGB4 in the presence of CHIR and PD or XL (Fig. 7J) were low compared with CHIR withdrawal (Fig. 4B), whereas NGFR was never detected (not shown). Taken together, these observations show that primarily distal fates were enhanced by cell cycle inhibition in the presence of CHIR. To morphologically assess maturation in CHIR+ cultures in the presence of cell cycle inhibitors, we performed TEM of CHIR+/PD and CHIR+/XL cultures. These studies revealed predominant presence of cells with LBs. However, these were not mature, and most appeared as multivesicular bodies (Fig. 7K). Similar to CHIR withdrawal, cell cycle inhibition therefore induced differentiation, but, in contrast to CHIR withdrawal, strongly favored distal cells and, in particular, the ATII lineage without promoting full maturation. We conclude that, cell cycle lengthening plays a role in the differentiation-inducing effect of CHIR withdrawal, but does not fully explain its effect on multilineage differentiation and maturation.

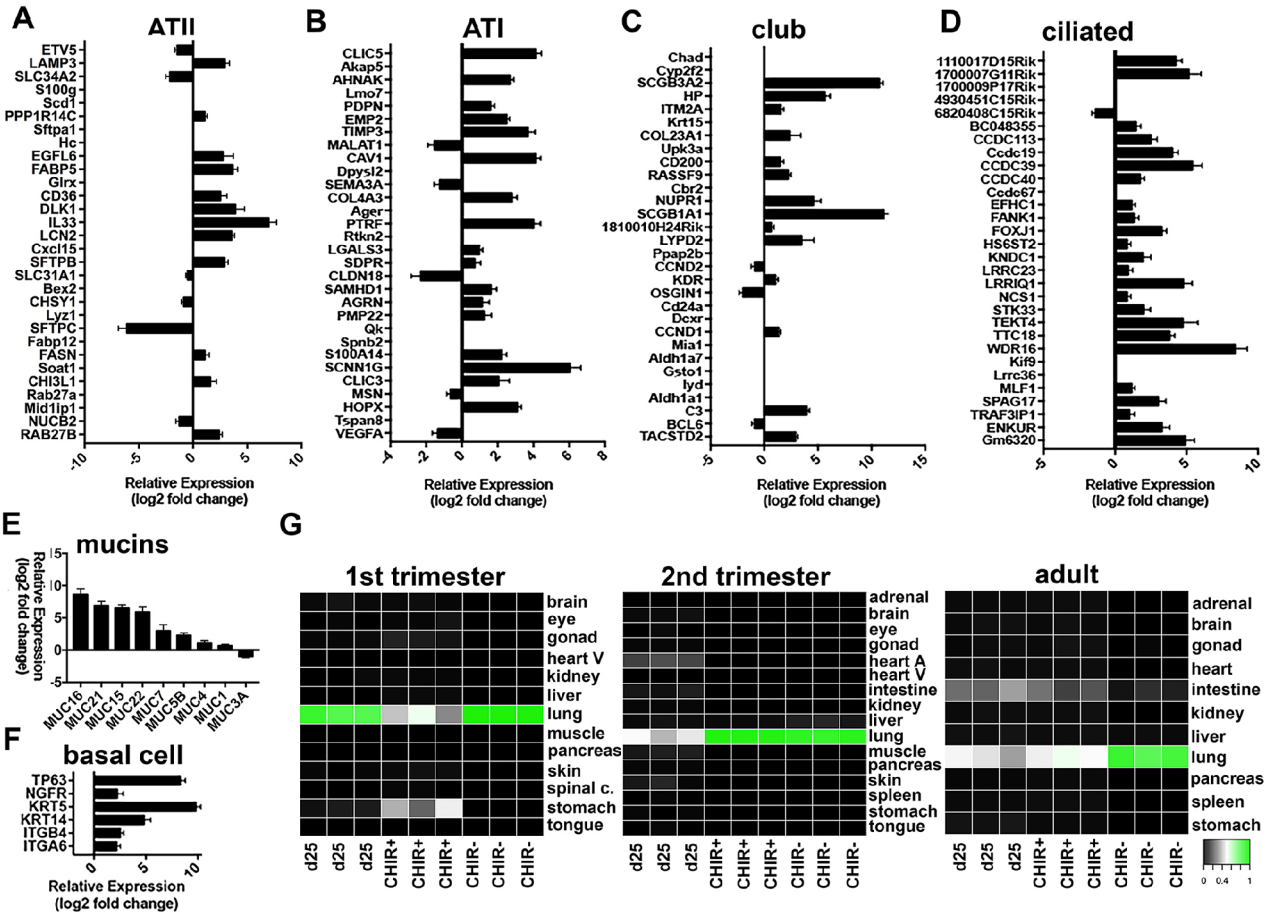

Fig. 5. Genome-expression analysis. (A-D) Genes significantly differently expressed by RNAseq in CHIR– compared with CHIR+ cultures classified as marking ATII, ATI, ciliated and club cell markers according to Treutlein et al. (2014). Data are shown for only the genes classified by Treutlein et al. (2014) as being significantly different between CHIR– and CHIR+ conditions. (E) Mucin genes significantly differently expressed by RNAseq in CHIR– compared with CHIR+ cultures. (F) Genes expressed in BCs significantly differently expressed by RNAseq in CHIR– compared with CHIR+ cultures (data are mean±s.d., *n*=3 independent experiments, all data shown FDR<0.05). (G) Comparison of genome-wide expression of LPs (d25), and d50 CHIR+ and CHIR– cultures using the KeyGenes database (*n*=3 independent experiments).

Development (2019) 146, dev171652. doi:10.1242/dev.171652

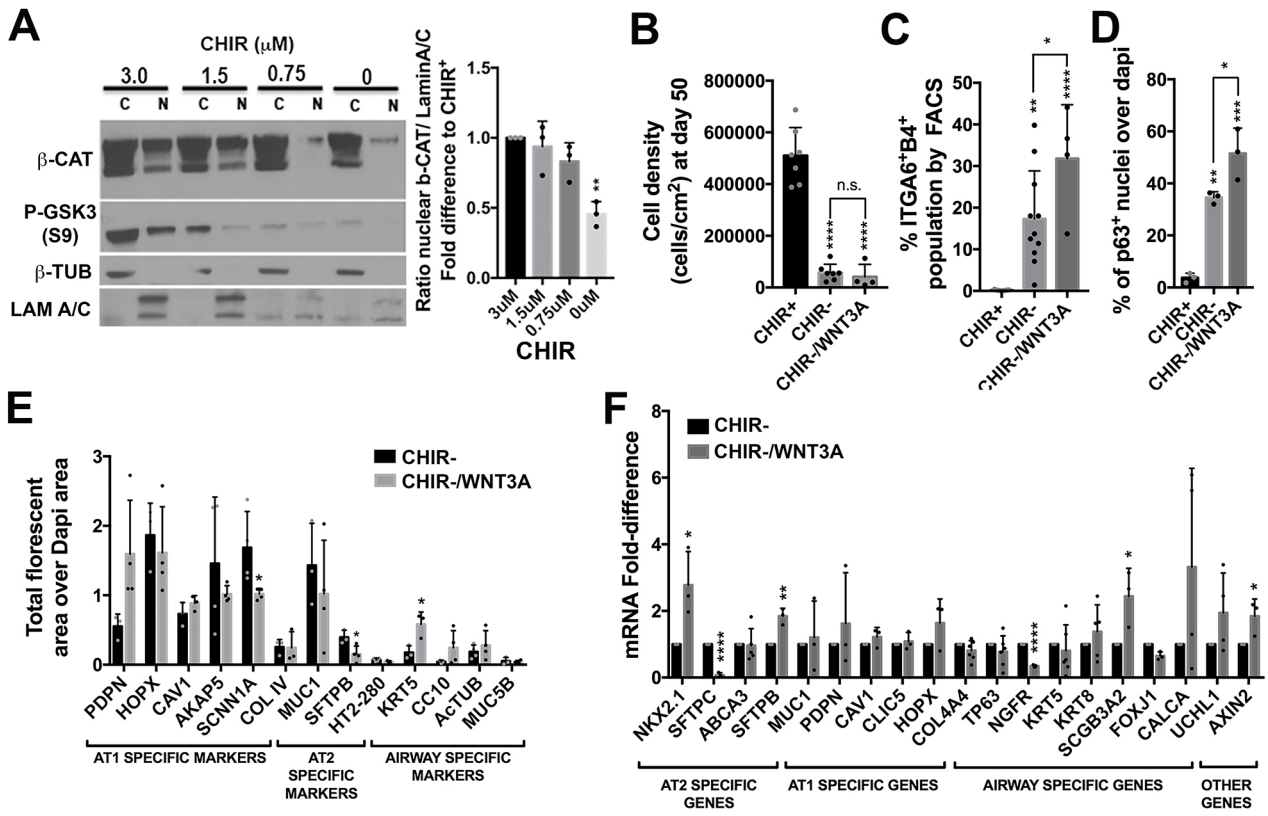

Fig. 6. Role of WNT signaling in the effect of CHIR. (A) Western blotting of nuclear and cytoplasmic fractions for β-catenin and S9 phospho-GSK3 in cultures treated with varying concentration of CHIR (representative of three experiments) and quantification of western blots of nuclear fractions of cultures treated with varying concentration of CHIR for nuclear β-catenin (data are mean±s.d., n=3 independent experiments, $^{**}P$<0.01). (B) Cell density in CHIR+, CHIR− and CHIR− cultures treated with 100 ng/ml WNT3A (data are mean± s.d.; CHIR+ and CHIR−, n=7; CHIR−/WNT3A, n=4 independent experiments; $^{****}P$<0.0001). (C) Fraction of ITGA6$^+$ITGB4$^+$ cells in CHIR+, CHIR−, and CHIR− cultures treated with 100 ng/ml WNT3A as determined by flow cytometry (data are mean±s.d.; CHIR+ and CHIR−, n=11; CHIR−/WNT3A, n=4 independent experiments; $^{*}P$<0.05, $^{**}P$<0.01, $^{****}P$<0.0001). (D) Fraction of P63$^+$ cells in CHIR+, CHIR− and CHIR− cultures treated with 100 ng/ml WNT3A, as determined by immunofluorescence (data are mean±s.d.; n=3 independent experiments; $^{*}P$<0.05, $^{**}P$<0.01, $^{***}P$<0.001). (E) Relative quantification of immunofluorescence for non-nuclear protein, as determined by the ratio between fluorescent area for a given marker and nuclear DAPI area in CHIR− cultures and CHIR− cultures treated with 100 ng/ml WNT3A (data are mean±s.d.; n=4 independent experiments; $^{*}P$<0.05). (F) Expression of mRNA for differentiation markers in CHIR− cultures treated with 100 ng/ml WNT3A relative to CHIR− (data are mean±s.d.; n=3-6 independent experiments; $^{*}P$<0.05, $^{**}P$<0.01, $^{****}P$<0.0001, see Table S4 for exact number of replicates per gene).

NOTCH regulates proximodistal specification

Several mouse genetic models suggest a role for NOTCH signaling in proximodistal specification, although, depending on the model, conflicting results have been reported (Xu et al., 2012). We therefore used our *in vitro* multilineage differentiation model to investigate whether and how NOTCH signaling affects the balance between proximal and distal cells.

In CHIR− cultures, several NOTCH receptors, NOTCH targets (Fig. 8A) and the NOTCH1 intracellular domain (NICD) (Fig. 8B) were upregulated compared with CHIR+ cultures, indicating that CHIR inhibits NOTCH signaling or that CHIR withdrawal induced a population that is subject to NOTCH signaling. To examine the role of NOTCH signaling in CHIR− cultures, we added the γ-secretase inhibitor DAPT. RT-qPCR (Fig. 8C) showed that inhibiting NOTCH in CHIR− cultures induced TP63, as well as neuroendocrine (CALCA, UCHL1) and ciliated (FOXJ1) markers, while profoundly repressing club cell (SCGB3A2) and distal markers, in particular ATII markers such as SFTPC and SFTPB (Fig. 8C). Phenotypic analysis showed a modest reduction in cell number (Fig. 8D), but an increase in the fraction of P63$^+$ nuclei (53.6±4.31%) (Fig. 8E) and of ITGA6$^+$ITGB4$^+$ cells, which made up 45±10.5% of the population (Fig. 8F). Immunofluorescence (Fig. S1, Fig. 8G) confirmed these findings. Therefore, NOTCH inhibition induced further differentiation of a select set of airway cells at the expense of other fates, including ATII fate, indicating a role for NOTCH signaling in proximodistal specification.

As inhibition of Rho-associated kinase (ROCK) facilitates culture of epithelial progenitors (Butler et al., 2016; Mou et al., 2016) and as DAPT promoted select proximal fates, we combined DAPT with the ROCK inhibitor (RI) Y27632. This resulted in a marked increase in cell number (Fig. 8H), 57.4±14.46% of which were P63$^+$ (Fig. 8I), and in ITGA6$^+$ITGB4$^+$ cells (1.17±0.5×10^5 cells cm^{-2}) (Fig. 8J,K). At d80, when ITGA6$^+$ITGB4$^+$ made up 77.8±2.3% of the population, only a minor fraction (8.1±0.8%) expressed the mature BC marker NGFR (Fig. 8L), suggesting that the ITGA6$^+$ITGB4$^+$ cells are in fact differentiating BCs. This notion is supported by the finding that DAPT and RI synergistically increased the number of ciliated cells in the cultures at d50 (Fig. 8M), and that this number increased further at d80 (Fig. 8N). These cells had numerous long cilia (Fig. 8O) confirmed by TEM (Fig. 8P) and by high-speed live imaging (Movies 1 and 2). Taken together, these findings indicate a roadmap for the generation of proximal progenitors and ciliated cells from LPs through removal of CHIR followed by inhibition of both NOTCH and ROCK signaling.

Development (2019) 146, dev171652. doi:10.1242/dev.171652

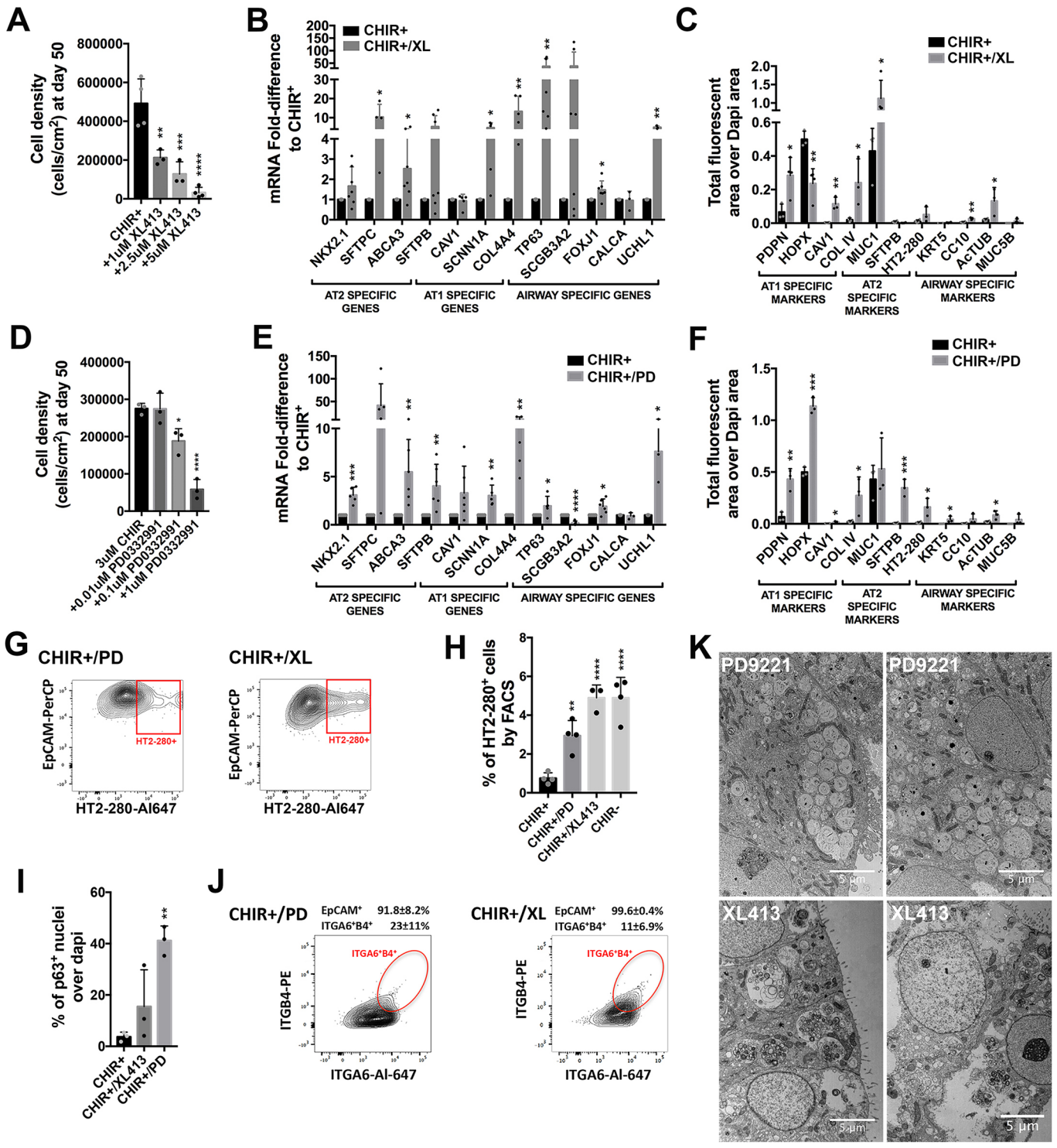

Fig. 7. See next page for legend.

Reproducibility in iPS lines

To ascertain the general validity of our observations made using RUES2 ESCs, we reproduced key findings in two iPS lines (Fig. S7). In both lines, CHIR removal inhibited cellular expansion (Fig. S7A,B) and induced a wide array of markers of differentiating cells (Fig. S7C,D). Furthermore, addition of DAPT and RI to CHIR − cultures strongly increased the absolute number (Fig. S7E) and the fraction (Fig. S7F) of ITGA6^{+}ITGB4^{+} cells. Both iPS lines therefore behaved similarly to RUES2 ESCs.

DISCUSSION

We describe here a method to differentiate LPs into the most mature lung and airway epithelial cells reported yet by culture in Col I 3D media in the absence of GSK3i. Neither NGFR^{+} BCs nor ATI cells that are morphologically recognizable as such were ever generated *in vitro*, although the lack of expression AGER on ATI suggests that these are still not fully mature. Importantly, in contrast to previous reports (Jacob et al., 2017; McCauley et al., 2017), this approach does not require reporter lines to isolate LPs or to identify specific lineages.

Development (2019) 146, dev171652. doi:10.1242/dev.171652

Fig. 7. Effect of cell cycle inhibition on lung progenitor maturation. (A) Cell density in CHIR+ cultures supplemented with increasing concentrations of the CDC7 inhibitor XL413 (data are mean±s.d.; *n*=3 independent experiments; ***P*<0.01, ****P*<0.001, *****P*<0.0001). (B) Expression of mRNA for differentiation markers in CHIR+ cultures treated with 5 µM of XL413 relative to CHIR+ cultures (data are mean±s.d.; *n*=3-7 independent experiments; **P*<0.05, ***P*<0.01, see Table S4 for the exact number of replicates per gene). (C) Relative quantification of immunofluorescence for non-nuclear protein as determined by the ratio between fluorescent area for a given marker and nuclear DAPI area in CHIR+ cultures and CHIR+ cultures treated with treated with 5 µM of XL413 (data are mean±s.d.; *n*=4 independent experiments; **P*<0.05, ***P*<0.01). (D) Cell density in CHIR+ cultures supplemented with increasing concentrations of the CDK4/6 inhibitor PD0339221 (data are mean±s.d.; *n*=3 independent experiments; **P*<0.05, *****P*<0.0001). (E) Expression of mRNA for differentiation markers in CHIR+ cultures treated with 1 µM of PD0332991 relative to CHIR+ cultures (data are mean±s.d., *n*=3-6 independent experiments; **P*<0.05, ***P*<0.01, ****P*<0.001, *****P*<0.0001, see Table S4 for exact number of replicates per gene). (F) Relative quantification of immunofluorescence for non-nuclear protein as determined by the ratio between fluorescent area for a given marker and nuclear DAPI area in CHIR+ cultures and CHIR+ cultures treated with 1 µM of PD0332991 (data are mean ±s.d.; CHIR+, *n*=4; CHIR+/PD, *n*=3 independent experiments; **P*<0.05, ***P*<0.01, ****P*<0.001). (G) Representative example of the flow cytometric profile after staining for EPCAM and HT2-280 of cells from CHIR+ cultures in the presence of either PD0332991 or XL413 (*n*=4 independent experiments). (H) Frequency of HT2-280$^+$ cells in CHIR+, CHIR– and CHIR+ cultures supplemented with either PD0332991 or XL413 (data are mean± s.d., CHIR+, CHIR– and CHIR+/PD, *n*=4; CHIR+/XL413, *n*=3 independent experiments; ***P*<0.01, *****P*<0.0001 compared with CHIR+). (I) Fraction of P63$^+$ cells in CHIR+ cultures in the presence of either PD0332991 or XL413, as determined by immunofluorescence (data are mean±s.d.; *n*= 3 independent experiments; ***P*<0.01). (J) Representative example and statistical analysis of the flow cytometric profile after staining ITGA6 and ITGB4 of cells from CHIR+ cultures in the presence of either PD0332991 or XL413 hydrochloride (gated on EPCAM+ cells, *n*=4 independent experiments). (K) Representative transmission electron micrograph images of CHIR+ cultures treated with 5 µM of XL413 or 1 µM PD0332991, showing cells with multiple big immature lamellar bodies and multivesicular bodies (representative of one experiment). Scale bars: 5 µm.

Our observations indicate that GSK3, a kinase that integrates multiple inputs and affects a wide variety of signaling pathways and cellular process (Patel and Woodgett, 2017), is a pivotal node in the regulation of the differentiation of LPs that appears to be at least partially independent from its effect on WNT signaling. The generation of embryonic lung progenitors (LPs) from AFE requires WNT signaling *in vitro* (Huang et al., 2014; Ostrin et al., 2018) and *in vivo* (Goss et al., 2009), which is stimulated *in vitro* by addition of the small molecular GSK3 inhibitor CHIR99021 (An et al., 2010). Continued presence of CHIR promoted cellular expansion and inhibited multilineage differentiation. Although canonical WNT signaling inhibits GSK3 Ser/Thr kinase activity, thereby stabilizing β-catenin (Willert and Nusse, 2012), the effect of CHIR could not be qualitatively recapitulated by a canonical WNT ligand, WNT3A. In fact, the canonical WNT ligand promoted a proximal fate, whereas CHIR repressed both proximal and distal maturation. Although WNT3A may be less active than CHIR with respect to activation of canonical WNT signaling in human cells (Fuerer and Nusse, 2010), rhWNT3A did induce the WNT target AXIN2 as well as nuclear β-catenin, indicating biological activity. Furthermore, as the effect of CHIR was dose dependent, a threshold effect of WNT signaling is unlikely. The effect of GSK3 could therefore not be assigned to a single signaling pathway. Part of the effect of CHIR may involve enhancement of cell cycling, one of the integrated outputs of GSK3, in particular for distal fates. This is consistent with the notion that GSK3 is a central node that integrates multiple inputs and regulates a broad range of downstream processes, including cell cycle (Patel and Woodgett, 2017). Similar observations were made in radial glia during brain development, where cell cycle inhibition favored differentiation at the expense of self-renewal (Calegari et al., 2005; Calegari and Huttner, 2003; Kim et al., 2009; Lange et al., 2009; Roccio et al., 2013). It is also clear, however, that mere cell cycle inhibition does not reproduce all effects of CHIR withdrawal, as CHIR withdrawal induced much more pronounced proximal differentiation, as well as morphologically more advanced ATII maturation.

Our findings appear at odds with reports showing that timed removal of CHIR from LPs promoted a proximal fate (McCauley et al., 2017), that its continued presence drove an ATII fate (Jacob et al., 2017) and that these effects were explained by attenuation or agonism of WNT signaling, respectively (Jacob et al., 2017; McCauley et al., 2017). In our Col I 3D model, WNT3A in fact induced a proximal and club cell fate. This is the opposite of the findings of Jacob et al. (2017) and McCauley et al. (2017), who used Matrigel to read out terminal cell fate. Although Col I is more permissive than Matrigel for the development of a broad array of lung and airway lineages, we obtained qualitatively similar data in Matrigel. A difference in the 3D media used can therefore not fully explain this discrepancy. McCauley et al. (2017) withdrew CHIR as early as d15, at the early LP stage. However, we observed that, at that stage, the cells were not yet fully competent to differentiate in 3D culture after CHIR withdrawal, a finding consistent the observations of Ostrin et al. (Ostrin et al., 2018). We furthermore also found that CHIR withdrawal at d35 had a similar effect to withdrawal at d25. Our studies therefore indicate that this discrepancy is not explained by different timing of CHIR withdrawal. McCauley et al. (2017) and Jacob et al. (2017) used reporter lines and cell sorting to isolate LPs from early-stage low-purity cultures, and withdrew CHIR in 2D culture prior to reading out proximal (McCauley et al., 2017) or distal fate (Jacob et al., 2017) in Matrigel spheroid cultures, under conditions that are selective for one or the other fate. In contrast, we did not perform cell sorting and withdrew CHIR after plating in Col I. This may be important, as we observed that, during prolonged 2D culture, detachment of cells occurs, which may, depending on culture conditions, affect some cell types more than others (Huang et al., 2015). Furthermore, to identify distal potential Jacob et al. (2017) first isolated SFTPC-reporter positive cells, which are already committed to the ATII lineage. It therefore appears logical that only ATII cells are detected in subsequent 3D cultures. Interestingly, however, Jacob et al. (2017) did report that withdrawal of CHIR in Matrigel cultures of ATII progenitors induced maturation, a finding that may be consistent with our observation that CHIR withdrawal induces multilineage differentiation, including differentiation of morphologically mature ATII cells. These findings may also be consistent with the fact that Wnt signaling promotes proliferation of subset of ATII cells involved in late alveologenesis and alveolar repair (Frank et al., 2016; Nabhan et al., 2018; Zacharias et al., 2018). In addition, we have previously shown that even immature ATII cells take-up and recycle SFTPB (Chen et al., 2017; Huang et al., 2014). Surfactant recycling is therefore a functional characteristic that is likely acquired relatively early in ATII differentiation and is not an indicator of maturity.

We next performed studies to examine whether this model can be used to gain deeper insight into proximodistal specification. A canonical WNT ligand stimulated club cell generation, whereas NOTCH inhibition promoted proximal, neuroendocrine and ciliated fates at the expense of distal fates. Our observations on the effect of NOTCH on the induction of specific proximal fates is consistent

Development (2019) 146, dev171652. doi:10.1242/dev.171652

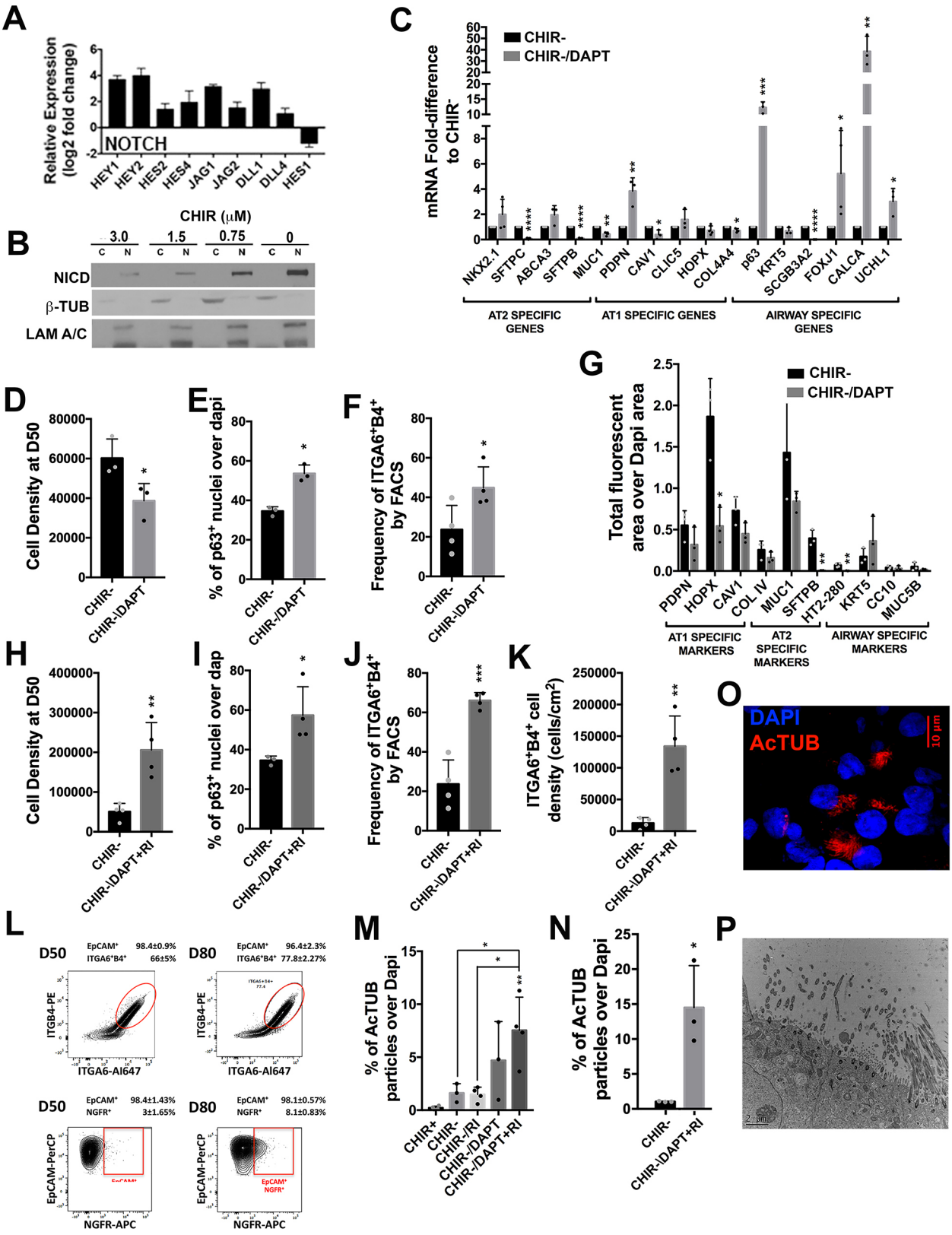

Fig. 8. See next page for legend.

with mouse genetic models (Mori et al., 2015; Rock et al., 2011; Tsao et al., 2008, 2009). We also found that NOTCH inhibition profoundly inhibited distal fates, thus indicating that active NOTCH promotes distal fate. The effect of NOTCH on proximodistal specification was not clear from mouse models, with some indicating inhibition of distal development (Tsao et al., 2008), and others showing the opposite (Dang et al., 2003; Guseh et al., 2009) or no effect (Xu et al., 2010) on distal development (Xu et al.,

Development (2019) 146, dev171652. doi:10.1242/dev.171652

Fig. 8. Effect of NOTCH inhibition on differentiation in CHIR− cultures. (A) NOTCH-related genes significantly differently expressed by RNAseq in CHIR− compared with CHIR+ cultures (data are mean±s.d., n=3 independent experiments; for all data shown, FDR<0.05). (B) Western blotting of nuclear and cytoplasmic fractions for NOTCH intracellular domain (NICD) in cultures treated with varying concentration of CHIR (representative of three experiments). (C) Expression of mRNA for differentiation markers in CHIR− cultures treated with 25 µM of DAPT relative to CHIR− cultures (data are mean±s.d., n=3 or 4 independent experiments; *P<0.05, **P<0.01, ***P<0.001, ****P<0.0001, see Table S4 for the exact number of replicates per gene). (D-F) Cell density (D), fraction of P63+ (E) and ITGA6$^+$ITGB4$^+$ (F) cells in CHIR− and CHIR− cultures treated with 25 µM of DAPT (data are mean±s.d.; D,E, n=3; F, n=4 independent experiments; *P<0.05). (G) Relative quantification of immunofluorescence for non-nuclear protein, as determined by the ratio between fluorescent area for a given marker and nuclear DAPI area in CHIR− cultures and CHIR− cultures treated 25 µM DAPT (data are mean±s.d.; n=3 independent experiments; *P<0.05, **P<0.01). (H-K) Cell density (H), fraction of P63$^+$ (I) and ITGA6$^+$ITGB4$^+$ (J) cells, and absolute number of ITGA6$^+$ITGB4$^+$ cells (K) in CHIR− and CHIR− cultures treated with 25 µM DAPT and 10 µM ROCK inhibitor (RI) (data are mean±s.d.; n=4 independent experiments; *P<0.05, **P<0.01, ***P<0.001). (L) Representative example and statistical analysis of the flow cytometric profile after staining for EPCAM, ITGA6, ITGB4 and NGFR of cells from d50 and d80 CHIR− cultures with 25 µM DAPT and 10 µM RI (n=4 independent experiments). (M) Fraction of AcTUB$^+$ clusters relative to DAPI in d50 CHIR+, CHIR− and CHIR− cultures treated with 25 µM DAPT and/or 10 µM RI (data are mean±s.d., CHIR+, CHIR−/RI and CHIR-/DAPT+RI, n=3; CHIR− and CHIR−/DAPT, n=4 independent experiments; *P<0.05, **P<0.01). (N) Fraction of AcTUB$^+$ clusters relative to DAPI in d80 CHIR− cultures with or without 25 µM DAPT and 10 µM RI (data are mean±s.d.; n=3 independent experiments; *P<0.05). (O) Representative confocal image of AcTUB in CHIR− culture supplemented with 25 µM DAPT and 10 µM RI (representative of four independent experiments). (P) Transmission electron microscopy image (representative of one experiment) of a cluster of ciliated cells in CHIR− culture supplemented with 25 µM DAPT and 10 µM RI. Scale bars: 10 µm in O; 2 µm in P.

2012). NOTCH was furthermore synergistic with ROCK inhibition in this respect. This was surprising, as it has been suggested that RI conditionally immortalizes a variety of epithelial progenitors by suppressing non-canonical NOTCH signaling pathways (Yugawa et al., 2013). Collectively, our observations show that this model provides novel mechanistic insight into human lung development that complements mouse genetic models, and it begins to provide a roadmap for the generation of specific lung and airway lineages.

MATERIALS AND METHODS

hPSC maintenance

RUES 2 (Rockfeller University Embryonic Stem Cell Line 2, NIH approval number NIHhESC-09-0013, registration number 0013; passage 17-28), Sendai Virus and modified mRNA-generated human dermal fibroblast iPSC lines (from healthy fibroblasts, purchased from Mount Sinai Stem Cell Core Facility, passage 17-26) were cultured on mouse embryonic fibroblasts (GlobalStem) plated at 17,000-20,000 cells cm^{-2}. hPSC maintenance media consisted of DMEM/F12 (Cellgro) 20% Knockout Serum Replacement (Gibco), 0.1 mM β-mercaptoethanol (Sigma-Aldrich), 1% GlutaMax (Gibco), 1% non-essential amino acids (Gibco), 0.2% primocin (InvivoGen) and 20 ng ml^{-1} FGF-2 (R&D Systems). Media were changed daily and cells were passaged every 4 to 5 days using Accutase/EDTA (Innovative Cell Technologies) at 1:24 dilution. Cells were maintained in an undifferentiated state in a humidified 5% CO_2 atmosphere at 37°C. The cells are tested for Mycoplasma contamination by PCR every 6 months. Karyotype was verified in 2016, and all cells used are low passages from that batch of lines.

Serum-free differentiation media

All differentiations were carried out in serum-free media consisting of IMDM/Ham's F12 (3:1) (Cellgro), N2 and B27 supplements (Gibco), 1% GlutaMax, 1% penicillin-streptomycin (Cellgro) and 0.05% bovine serum albumin (BSA) (Gibco). Ascorbic acid (50 µg ml^{-1}; Sigma-Aldrich), 0.4 µM monothioglycerol (Sigma-Aldrich) and the indicated growth factors were added fresh.

Definitive endoderm induction [days 1-4 differentiation protocol (dp)]

hPSCs were dissociated with Accutase/EDTA for 3 min at 37°C into small 3- to 10-cell clumps and plated on low-attachment 6-well plates at 120,000-150,000 cells cm^{-2} to form embryoid bodies (EBs) in serum-free differentiation (SFD) media supplemented with 100 ng ml^{-1} activin A (R&D Systems), 10 µM of ROCK inhibitor (RI) Y-27632 (Tocris), 0.5 ng ml^{-1} BMP4 (R&D Systems) and 2.5 ng ml^{-1} FGF2 (R&D Systems) for 72 h at 37°C in 5% CO_2/5% O_2/95% N_2 atmosphere. Complete media changes were performed every 24 h. Endoderm induction efficiency was determined by the percentage of cells double-positive for CXCR4 and KIT by flow cytometry as previously described (Huang et al., 2015, 2014) after dissociation of EBs with 0.05% trypsin/EDTA (Gibco). Typically, experiments with endoderm efficiencies of ≥98% CXCR4$^+$KIT$^+$ cells for RUES2 and ≥90% CXCR4$^+$KIT$^+$ cells for Sendai virus and mRNA-generated iPSCs were taken through the next steps of the differentiation protocol.

Anterior foregut endoderm induction (days 4-6 dp)

Anterior foregut endoderm induction (AFE) was carried out as previously described (Huang et al., 2014, 2015). Briefly, EBs were dissociated to single cells with 0.05% trypsin/EDTA for 5 min and plated at 50,000-75,000 cells cm^{-2} in 0.33% fibronectin (R&D Systems)-coated 24-well plates in SFD media supplemented with 2 µM dorsomorphin (Tocris) and 10 µM SB431542 (Tocris) for the first 24 h followed by SFD supplemented with 1 µM IWP2 (Tocris) and 10 µM SB431542 for another 24 h. Differentiation was carried out at 37°C in 5% CO_2/5% O_2/95% N_2 atmosphere.

Lung progenitor specification (days 6-15 dp)

Lung progenitor (LPs) specification was carried out as previously described (Huang et al., 2014, 2015). Briefly, a media switch was performed following the 48 h of AFE induction to SFD plus the lung factors 3 µM CHIR99021 (Tocris), 10 ng ml^{-1} FGF7 (R&D Systems), 10 ng ml^{-1} FGF10 (R&D Systems), 10 ng ml^{-1} BMP4 and 50 nM all-trans retinoic acid (R&D Systems). Complete media changes were performed every 48 h and cells were maintained at 37°C in 5% CO_2/5% O_2/95% N_2 atmosphere for the first 2-3 days in lung factor media and then switched to a 5% CO_2 atmosphere at 37°C.

Expansion of LPs (days 15-25 dp)

At d15 of the differentiation protocol, cells were briefly trypsinized for 1 min at 37°C and replated into 24-well growth factor-reduced Matrigel-coated (Corning; 1:100 dilution) plates at 1:2 splitting ratio. LPs were expanded in SFD plus 3 µM CHIR99021, 10 ng ml^{-1} FGF7 and 10 ng ml^{-1} FGF10, with media changes every 48 h and in 5% CO_2 atmosphere at 37°C. At d25, experiments were accessed for LP generation efficiency by immunofluorescence staining for NKX2.1, SOX2 and FOXA1 as previously described (Huang et al., 2014, 2015). Typically, experiments with ≥90% NKX2.1$^+$SOX2$^+$FOXA1$^+$ cells for RUES2 and with ≥80% NKX2.1$^+$SOX2$^+$FOXA1$^+$ cells for Sendai virus and mRNA-generated iPSCs were carried further.

LP maturation in collagen I gels (days 25-50 dp)

At d25 of the differentiation protocol, cells were briefly trypsinized for 1 min at 37°C. Cells were scraped off the plate and cell clumps collected and re-suspended in a 4.5 mg ml^{-1} rat tail collagen I (Col I) (Trevigen) solution prepared according to the manufacturer's gelation protocols. An equivalent of 100,000 cells cm^{-2} in cell clumps were plated in 24- or 48-well plates and placed at 37°C 10-15 min for gelation. Medium was added on top of the gels and changed every 48 h. Maturation media consisted of SFD plus 10 ng ml^{-1} FGF7, 10 ng ml^{-1} FGF10, 50 ng ml^{-1} dexamethasone (Tocris), 0.1 mM 8-bromo-cAMP (Tocris) and 0.1 mM IBMX (Tocris) (CHIR−). When indicated, CHIR99021 was included in the maturation media (CHIR+) (3 µM). For some experimental conditions, other factors or small molecules were added to the media: 25 µM DAPT (Tocris), 10 µM Y-27632 (RI), 100 ng ml^{-1} WNT3A (R&D Systems), 1 µM PD0332991

Development (2019) 146, dev171652. doi:10.1242/dev.171652

(Tocris) and 5 µM XL413 hydrochloride (Tocris). Cells were maintained in a 5% CO_2 atmosphere at 37°C.

Timed CHIR withdrawal

For experiments in which CHIR was retracted at d15, d15 LPs were briefly trypsinized for 1 min at 37°C. Cells were scraped off the plate, and cell clumps collected and re-suspended in 4.5 mg ml^{-1} rat tail Col I solution at an equivalent of 100,000 cells cm^{-2} in cell clumps plated in 48-well plates and placed at 37°C for 10-15 min for gelation. Cultures were maintained in CHIR+ or CHIR− differentiation media, as described in the previous section, until d50. For experiments in which CHIR was withdrawn at d35, 3D cultures were established as described above at d25 and maintained in CHIR+ media until d35, after which CHIR was retracted and cultures maintained in CHIR− maturation media until d50.

LPs maturation in Matrigel 3D media

d25 LPs were briefly trypsinized and scraped off the tissue culture plate as described above. An equivalent of 100,000 cells cm^{-2} in cell clumps were suspended in Matrigel 3D media and plated in 48-well plates. After polymerization at 37°C, cultures were maintained in CHIR+ or CHIR− differentiation media as described above until d50. For cultures maintained in CHIR− FGF2 maturation media, SFD was supplemented with 250 ng ml^{-1} FGF2, 100 ng ml^{-1} FGF10, 50 ng ml^{-1} dexamethasone, 0.1 mM 8-bromo-cAMP and 0.1 mM IBMX.

Human lung tissue

Human fetal lung samples were purchased from Advance Bioscience Resources. Adult lung samples were obtained from lungs rejected for transplantation procured from the LiveOnNY (Live On New York) organ procurement organization, under a protocol approved by the Institutional Review Board at Columbia University.

Immunofluorescence

Col I gels, Matrigel 3D cultures and human lung samples were embedded in OCT and sectioned into 6 µm slices placed on microscopic slides. Slices were briefly fixed with 95% ethanol for 1 min at room temperature followed by 4% paraformaldehyde for 15 min at room temperature. After washing twice with PBS, slices were permeabilized with 0.25% triton in blocking buffer [5% donkey serum (EMD Millipore) in PBS] for 10 min at room temperature and blocked for 1 h at room temperature in blocking buffer. Primary antibodies diluted in blocking buffer were incubated at 4°C overnight. The following day, slices were washed twice with PBS, and secondary antibodies (Jackson ImmunoResearch) (Invitrogen) diluted in blocking buffer were incubated for 2 h at room temperature followed by a 5 min incubation with DAPI in PBS and two washes with PBS. Slides were mounted with ProLong Gold antifade reagent (Invitrogen) sealed and preserved in dark at 4°C. A complete list of antibodies and dilutions used can be found in Table S2. Antibodies were validated in archival human adult and fetal lung samples.

Air-liquid interphase (ALI) cultures were fixed with 4% paraformaldehyde for 15 min at room temperature prior to embedding in OCT and sectioned into slides. Sorted ITGA6$^+$ITGB4$^+$ cells were plated into Col I-coated glass-bottom plates, spun down at 70 ***g*** and left for 1 h at 37°C to adhere before being fixed and stained as described above.

Samples were imaged using a motorized Leica DMI6000 B or DMi8 inverted microscope and processed using ImageJ software. For high-magnification images, we used an IX83 Andor Revolution XD Spinning Disk Confocal System with a 100× oil objective (NA 1.49) and a 2× magnifier coupled to an iXon Ultra 888 EMCCD Camera.

Immunofluorescence quantification

For each marker, tile scans corresponding to the whole cross section area were acquired and quantified using ImageJ software. For transcription factors, images were converted to 8-bit and threshold values were determined to cover nuclear area. The number of positive particles (positive nuclei) was determined using the 'Analyze Particles' function of ImageJ. The percentage of positive cells was calculated by dividing the number of positive particles by the total number of DAPI-stained particles (total number of nuclei). For cytoplasmic and membrane markers, total positive (fluorescent) area was calculated by converting the image to 8-bit and thresholding it to the value that best covered the stained area. Fluorescent area was determined using the 'Analyze Particles' function. Total fluorescent area was then normalized to total DAPI-stained area.

Quantitative real-time PCR

d50 cultures in Col I gels were digested with 150 U ml^{-1} collagenase type I in IMDM for 45 min at 37°C, while cells cultured in Matrigel were retrieved using Cell Recovery Solution (Corning). Cells were collected and total RNA was extracted using RLT buffer and RNeasy Micro Kit (Qiagen). RNA concentration was measured using a NanoDrop 2000 fluorospectrometer (Thermo Fisher Scientific). cDNA was generated by reverse transcription of 1 µg of total RNA with random hexamers and Superscript III (Invitrogen) following the manufacturer's instructions. Real-time quantitative PCR was performed using the ABI Power SYBR green PCR Master Mix (Applied Biosystems) on an ABI vii7A Thermocycler (Applied Biosystems) with the following amplification conditions: 50°C for 2 min and 95°C for 10 min, followed by 40 cycles of 95°C for 15 s and 60°C for 1 min, plus dissociation/melt curves. Real-time quantitative PCR was performed on three biological samples from each experiment with technical triplicates for each sample. cDNA input per reaction was 5 ng. Analysis was performed using the standard curve method: for each gene, absolute quantification was obtained using a standard curve of serial diluted genomic DNA and normalized to the housekeeping gene TBP (TAT box-binding protein), then fold-differences were calculated to designated calibrator sample (CHIR$^+$ or CHIR$^-$ conditions). Primer sequences used can be found in Table S3.

Flow cytometry

Col I gels were digested with 150 U ml^{-1} collagenase type I in IMDM for 45 min at 37°C. Cell colonies were collected and further dissociated with pre-warmed 0.05% Trypsin/EDTA for 5 min to single cells. Cells were incubated at 4°C for 45 min in PBS with 0.2% BSA and 2 mM EDTA with: (1) anti-EpCAM PerCP (Invitrogen), anti-ITGA6 Alexa Fluor 647 and anti-ITGB4 PE (BioLegend); (2) anti-EpCAM PerCP and anti-NGFR APC (BioLegend); or (3) anti-EpCAM and unconjugated HT2-280 antibody followed by anti-mouse IgM Alexa Fluor 647. Catalog numbers and dilutions are provided in Table S2. Stained cells were analyzed on BD LSRII and BD Fortessa Analyzers (BD Bioscience). Results were analyzed using Flowjo v10.2 software. Analysis was gated on live, doublet-excluded, EPCAM$^+$ cells.

Population isolation by FACS sorting

d50 cells were dissociated and stained for EPCAM, ITGA6 and ITGB4, as described above. Populations were sorted using a BD Influx cell sorter (BD Bioscience) into complete media.

NGFR$^+$ basal cell expansion and air-liquid interface cultures

Col I gels were digested with collagenase type I and cell clumps trypsinized to single cells, as described above. Single cells were stained using anti-human EpCAM-PerCP, anti-human ITGB4-PE and anti-human NGFR-APC for 45 min at 4°C in FACS buffer. EpCAM$^+$ITGB4$^+$NGFR$^+$ basal cells were sorted using a BD Influx cell sorter (BD Bioscience) into epithelial media (Butler et al., 2016). Sorted cells were seeded onto irradiated 3T3-J2 feeders and maintained in epithelial media over three passages. Passage 2 cells were used for air-liquid interface cultures. 200,000 cells were seeded onto Matrigel-coated (1:30) 0.33 cm^2 transwells and kept in epithelial media on the upper and lower chamber for the first 48 h, after which ALI was induced and cells maintained in PneumaCult-ALI media (Stem Cell Technologies).

Western blot

d50 cultures in Col I gels were digested with 150 U ml^{-1} collagenase type I in IMDM for 45 min at 37°C. Cell colonies were collected and further dissociated with pre-warmed 0.05% Trypsin/EDTA for 3-5 min to small cell clumps (≤10cells). Nuclear/cytosol cell fractionations were performed by lysing the cell pellets with a 2× volume of 10 mM HEPES (pH 8.0), 1.5 mM $MgCl_2$ solution with 1× protease inhibitors (Roche) and 1/10 volume of 3% NP-40 for 10 min on ice. Plasma membrane lysis was verified using Trypan

Development (2019) 146, dev171652. doi:10.1242/dev.171652

Blue staining. Lysate was spun at 21,000 ***g*** for 10 min at 4°C and the supernatant (cytoplasmic fraction) was collected. The remaining pellet was re-suspended in 1× volume of 20 mM HEPES (pH 8.0), 25% glycerol, 420 mM NaCl, 1.5 mM $MgCl_2$ and 0.2 mM EDTA solution with 1× protease inhibitors, incubated at 4°C for 1 h with rotation and spun at 21,000 ***g*** for 20 min at 4°C. Supernatant (nuclear fraction) was collected and diluted with 1× volume of 1.5 mM $MgCl_2$, 0.6% NP40 and 0.2 mM EDTA nuclear diluent solution. For each sample, 20 µg of protein corresponding to nuclear and cytosolic fractions were denaturated in 6× loading buffer at 95°C for 5 min and loaded onto separate lanes of 4-12% Bis-Tris SDS-PAGE gradient Gels (Invitrogen). Gels were transferred into a 0.22 µm nitrocellulose membrane and stained with Ruby Red (Molecular Probes) to confirm transfer. Membranes were blocked with 5% non-fat milk in TBS-Tween 0.05% and incubated with anti-cleaved NOTCH1, anti-β-catenin, anti-phospho-GSK3β (Ser9), anti-Lamin A/C and anti-β Tubulin antibodies overnight at 4°C with agitation. Membranes were washed, incubated with the appropriate HRP-conjugated secondary antibodies for 2 h at room temperature with agitation, washed again and exposed to X-ray film (Denville) after incubation with Pierce ECL Western Blotting Substrate or SuperSignal West Femto ECL reagent (Thermo Fisher Scientific). A complete list of antibodies and dilutions used can be found in Table S2.

RNA sequencing

Total RNA from d25 and d50 (after Col I digestion as described above) cultures was purified using RNeasy Micro Kit. Agilent microfluidic RNA 6000 Nano Chip Kit (Agilent Technologies) and 2100 Bioanalyser (Agilent Technologies) were used to determine RNA concentration and integrity number (RIN). All sequenced samples had a RIN≥9.5. Poly-A pull-down was used to enrich mRNAs from total RNA samples. Library preparation was performed using an Illumina TruSeq RNA prep kit. Libraries were then sequenced using an Illumina HiSeq2500 at Columbia Genome Center. Samples were multiplexed in each lane to yield targeted number of single-end 100 bp reads for each sample, as a fraction of 280-400 million reads for the whole lane. RTA (Illumina) was used for base calling and bcl2fastq2 (version 2.17) for converting BCL to fastq format, coupled with adaptor trimming. Reads were mapped to the human genome (NCBI/build37.2) using STAR(2.5.2b) and featureCounts (v1.5.0-p3). Differentially expressed genes under various conditions were tested using DEseq, an R package based on a negative binomial distribution that models the number reads from RNA-seq experiments and tests for differential expression.

Single cell RNA sequencing

d50 cultures in Col I were digested with collagenase type I as described above, followed by trypsinization with pre-warmed 0.05% Trypsin/EDTA until cultures were dissociated to single cells. The Chromium Single Cell 3′ Library & Gel Bead Kit v2, 16 rxns PN-120237 kit was used according to the manufacturer's instructions (10× Genomics). Five-thousand cells/library were targeted. Twelve cycles were used for cDNA amplification and for the sample index PCR. Libraries were pooled and sequenced to a depth of ∼350 M reads on an Illumina HiSeq 4000. The cellranger pipeline v2.0.0 (10× Genomics) was used to process the data and the reference genome was GRCh38.

KeyGenes analysis

Identity of d25 and d50 cultures were predicted by KeyGenes algorithm (Roost et al., 2015) from its transcriptional profile based on next-generation sequencing data of human fetal tissues from the first and second trimester of development, and adult tissues.

Transmission electron microscopy

TEM was performed at the NYULMC Microscopy Core Laboratory. Col I gels were fixed with 2.5% glutaraldehyde and 2% paraformaldehyde in 0.1 M sodium cacodylate buffer (pH 7.2) for 2 h and post-fixed with 1% osmium tetroxide for 1.5 h at room temperature, then processed in a standard manner and embedded in EMbed 812 (Electron Microscopy Sciences). Semi-thin sections were cut at 1 µm and stained with 1% Toluidine Blue to evaluate the quality of preservation and find the area of interest. Ultrathin sections (60 nm) were cut, mounted on copper grids and stained with uranyl acetate and lead citrate using standard methods. Stained grids were examined under Philips CM-12 electron microscope and photographed with a Gatan (4k ×2.7k) digital camera.

Light sheet microscopy

d50 cultures within the Col I gels were fixed overnight with 4% PFA, washed three times with PBS for 10 min and permeabilized with 0.25% triton in blocking buffer (5% donkey serum in PBS) for 4 h at room temperature with rotation. The gels were blocked with blocking buffer for 4 h at room temperature with rotation and then left incubating with primary antibodies overnight at 4°C with rotation. On the following day, the gels were washed three times with PBS for 10 min with rotation, incubated with the appropriate secondary antibodies for 4 h at room temperature with rotation followed by a 10 min incubation with DAPI in PBS and two 10 min washes with PBS at room temperature with rotation. 3D structures within the gel were dissected, mounted on agarose and imaged with the SP8-DLS system on a DMi8 inverted microscope, 2.5× illumination objectives with the 5 mm TwinFlect mirror fitted on the 10× detection objective (0.3 NA W DLS) (Leica-Microsystems) or the Zeiss Lightsheet Z.1 running ZEN 2014 SP1 (black edition) version 9,2, detection objective EC Plan-Neofluar 5×/0.16NA. Acquired images were then resized and 3D renderings were obtained using the 3D project function of ImageJ software.

Live imaging of d50 cultures

d50 cultures in Col I gels were digested with 150 U ml^{-1} collagenase type I (Gibco) in IMDM for 45 min at 37°C. Cell colonies were collected and further dissociated with pre-warmed 0.05% Trypsin/EDTA for 2-3 min to small sized cell clumps. Cells were re-suspended in SFD maturation media and plated in 50 mm glass-bottom dishes. Live imaging was performed using an IX83 Andor Revolution XD Spinning Disk Confocal System with an environmental chamber at 37°C and a 60× silicone oil objective (NA 1.30). Image acquisition was carried out using a Zyla 5.5. sCMOS camera (2048×2048 pixels) and the imaging software Metamorph.

Statistics and reproducibility

For statistical analysis between two groups, an unpaired two-tailed Student's *t*-test was used. For multiple group comparison, one-way ANOVA was performed followed by Dunnett or Tukey multiple comparison tests. Results are displayed as mean±s.d. with $P<0.05$ considered statistically significant. *n* values refer to biologically independent replicates. Grubbs and ROUT tests were used to exclude outliers. No blinding of investigators was used. No samples were *a priori* excluded.

Acknowledgements

We thank NYULMC OCS Microscopy core for their assistance with transmission electron microscopy. We thank NYULMC DART Microscopy Lab, Joseph Sall, Jessica Shivas, PhD and Albert E. Ayoub, PhD for their assistance in the light sheet microscopy work. We thank Dr Matthew Bacchetta for providing human adult lung samples. Flow cytometry was performed in the CCTI Flow Cytometry Core, supported in part by the Office of the Director, National Institutes of Health under awards S10RR027050 and S10OD020056.

Competing interests

The authors declare no competing or financial interests.

Author contributions

Conceptualization: H.-W.S., A.L.R.T.d.C; Methodology: H.-W.S., R.B.V.; Formal analysis: A.L.R.T.d.C., A.S.; Investigation: A.L.R.T.d.C., T.J.D., Y.-W.C., H.-Y.L.; Resources: H.-W.S.; Data curation: A.S., A.L.R.T.d.C; Writing - original draft: H.-W.S.; Writing - review & editing: H.-W.S., A.L.R.T.d.C.; Supervision: H.-W.S., J.C.-P.; Project administration: H.-W.S.; Funding acquisition: H.-W.S.

Funding

This work was supported by the National Institutes of Health (HL120046 and 1U01HL134760 to H.-W.S. and HD40182 to R.B.V.), the Thomas R Kully IPF Research Fund (H.-W.S.), the Fundação para a Ciência e a Tecnologia (PD/BD/52320/2013 to A.L.R.T.d.C. and the American Heart Association (T.J.D.). A.S. is a New York Stem Cell Foundation–Druckenmiller Fellow. Deposited in PMC for release after 12 months.

Data availability

The RNA sequencing and single cell RNA sequencing results have been deposited in GEO under accession number GSE101558. All data supporting the findings in this manuscript are available in Table S4.

Supplementary information

Supplementary information available online at
http://dev.biologists.org/lookup/doi/10.1242/dev.171652.supplemental

References

An, W. F., Germain, A. R., Bishop, J. A., Nag, P. P., Metkar, S., Ketterman, J., Walk, M., Weiwer, M., Liu, X., Patnaik, D. et al. (2010). *Discovery of Potent and Highly Selective Inhibitors of GSK3b*. In Probe Reports from the NIH Molecular Libraries Program. Bethesda, MD).

Butler, C. R., Hynds, R. E., Gowers, K. H., Lee, D. D. H., Brown, J. M., Crowley, C., Teixeira, V. H., Smith, C. M., Urbani, L., Hamilton, N. J. et al. (2016). Rapid expansion of human epithelial stem cells suitable for airway tissue engineering. *Am. J. Respir. Crit. Care. Med.* **194**, 156-168.

Calegari, F. and Huttner, W. B. (2003). An inhibition of cyclin-dependent kinases that lengthens, but does not arrest, neuroepithelial cell cycle induces premature neurogenesis. *J. Cell Sci.* **116**, 4947-4955.

Calegari, F., Haubensak, W., Haffner, C. and Huttner, W. B. (2005). Selective lengthening of the cell cycle in the neurogenic subpopulation of neural progenitor cells during mouse brain development. *J. Neurosci.* **25**, 6533-6538.

Chen, F., Cao, Y., Qian, J., Shao, F., Niederreither, K. and Cardoso, W. V. (2010). A retinoic acid-dependent network in the foregut controls formation of the mouse lung primordium. *J. Clin. Invest.* **120**, 2040-2048.

Chen, Y.-W., Huang, S. X., de Carvalho, A., Ho, S.-H., Islam, M. N., Volpi, S., Notarangelo, L. D., Ciancanelli, M., Casanova, J.-L., Bhattacharya, J. et al. (2017). A three-dimensional model of human lung development and disease from pluripotent stem cells. *Nat. Cell Biol.* **19**, 542-549.

Dang, T. P., Eichenberger, S., Gonzalez, A., Olson, S. and Carbone, D. P. (2003). Constitutive activation of Notch3 inhibits terminal epithelial differentiation in lungs of transgenic mice. *Oncogene* **22**, 1988-1997.

Dean, C. H., Miller, L.-A. D., Smith, A. N., Dufort, D., Lang, R. A. and Niswander, L. A. (2005). Canonical Wnt signaling negatively regulates branching morphogenesis of the lung and lacrimal gland. *Dev. Biol.* **286**, 270-286.

Desai, T. J., Brownfield, D. G. and Krasnow, M. A. (2014). Alveolar progenitor and stem cells in lung development, renewal and cancer. *Nature* **507**, 190-194.

Dickson, M. A. (2014). Molecular pathways: CDK4 inhibitors for cancer therapy. *Clin. Cancer Res.* **20**, 3379-3383.

Domyan, E. T., Ferretti, E., Throckmorton, K., Mishina, Y., Nicolis, S. K. and Sun, X. (2011). Signaling through BMP receptors promotes respiratory identity in the foregut via repression of Sox2. *Development* **138**, 971-981.

Dye, B. R., Hill, D. R., Ferguson, M. A., Tsai, Y. H., Nagy, M. S., Dyal, R., Wells, J. M., Mayhew, C. N., Nattiv, R., Klein, O. D. et al. (2015). In vitro generation of human pluripotent stem cell derived lung organoids. *eLife* **4**, e05098.

Dye, B. R., Dedhia, P. H., Miller, A. J., Nagy, M. S., White, E. S., Shea, L. D. and Spence, J. R. (2016). A bioengineered niche promotes in vivo engraftment and maturation of pluripotent stem cell derived human lung organoids. *eLife* **5**, e19732.

Firth, A. L., Dargitz, C. T., Qualls, S. J., Menon, T., Wright, R., Singer, O., Gage, F. H., Khanna, A. and Verma, I. M. (2014). Generation of multiciliated cells in functional airway epithelia from human induced pluripotent stem cells. *Proc. Natl. Acad. Sci. USA* **111**, E1723-E1730.

Frank, D. B., Peng, T., Zepp, J. A., Snitow, M., Vincent, T. L., Penkala, I. J., Cui, Z., Herriges, M. J., Morley, M. P., Zhou, S. et al. (2016). Emergence of a wave of Wnt signaling that regulates lung alveologenesis by controlling epithelial self-renewal and differentiation. *Cell Reports* **17**, 2312-2325.

Fuerer, C. and Nusse, R. (2010). Lentiviral vectors to probe and manipulate the Wnt signaling pathway. *PLoS ONE* **5**, e9370.

Gonzales, L. W., Guttentag, S. H., Wade, K. C., Postle, A. D. and Ballard, P. L. (2002). Differentiation of human pulmonary type II cells in vitro by glucocorticoid plus cAMP. *Am. J. Physiol.* **283**, L940-L951.

Goss, A. M., Tian, Y., Tsukiyama, T., Cohen, E. D., Zhou, D., Lu, M. M., Yamaguchi, T. P. and Morrisey, E. E. (2009). Wnt2/2b and beta-catenin signaling are necessary and sufficient to specify lung progenitors in the foregut. *Dev. Cell* **17**, 290-298.

Gotoh, S., Ito, I., Nagasaki, T., Yamamoto, Y., Konishi, S., Korogi, Y., Matsumoto, H., Muro, S., Hirai, T., Funato, M. et al. (2014). Generation of alveolar epithelial spheroids via isolated progenitor cells from human pluripotent stem cells. *Stem Cell Reports* **3**, 394-403.

Guseh, J. S., Bores, S. A., Stanger, B. Z., Zhou, Q., Anderson, W. J., Melton, D. A. and Rajagopal, J. (2009). Notch signaling promotes airway mucous metaplasia and inhibits alveolar development. *Development* **136**, 1751-1759.

Huang, S. X. L., Islam, M. N., O'Neill, J., Hu, Z., Yang, Y.-G., Chen, Y.-W., Mumau, M., Green, M. D., Vunjak-Novakovic, G., Bhattacharya, J. et al. (2014). Efficient generation of lung and airway epithelial cells from human pluripotent stem cells. *Nat. Biotechnol.* **32**, 84-91.

Huang, S. X., Green, M. D., de Carvalho, A. T., Mumau, M., Chen, Y.-W., D'Souza, S. L. and Snoeck, H.-W. (2015). The in vitro generation of lung and airway progenitor cells from human pluripotent stem cells. *Nat. Protoc.* **10**, 413-425.

Jacob, A., Morley, M., Hawkins, F., McCauley, K. B., Jean, J. C., Heins, H., Na, C. L., Weaver, T. E., Vedaie, M., Hurley, K. et al. (2017). Differentiation of human pluripotent stem cells into functional lung alveolar epithelial cells. *Cell Stem Cell* **21**, 472-488 e410.

Kim, W.-Y., Wang, X., Wu, Y., Doble, B. W., Patel, S., Woodgett, J. R. and Snider, W. D. (2009). GSK-3 is a master regulator of neural progenitor homeostasis. *Nat. Neurosci.* **12**, 1390-1397.

Konishi, S., Gotoh, S., Tateishi, K., Yamamoto, Y., Korogi, Y., Nagasaki, T., Matsumoto, H., Muro, S., Hirai, T., Ito, I. et al. (2016). Directed induction of functional multi-ciliated cells in proximal airway epithelial spheroids from human pluripotent stem cells. *Stem Cell Reports* **6**, 18-25.

Lancaster, M. A. and Knoblich, J. A. (2014). Organogenesis in a dish: modeling development and disease using organoid technologies. *Science* **345**, 1247125.

Lange, C., Huttner, W. B. and Calegari, F. (2009). Cdk4/cyclinD1 overexpression in neural stem cells shortens G1, delays neurogenesis, and promotes the generation and expansion of basal progenitors. *Cell Stem Cell* **5**, 320-331.

Li, Y., Gordon, J., Manley, N. R., Litingtung, Y. and Chiang, C. (2008). Bmp4 is required for tracheal formation: a novel mouse model for tracheal agenesis. *Dev. Biol.* **322**, 145-155.

Longmire, T. A., Ikonomou, L., Hawkins, F., Christodoulou, C., Cao, Y., Jean, J. C., Kwok, L. W., Mou, H., Rajagopal, J., Shen, S. S. et al. (2012). Efficient derivation of purified lung and thyroid progenitors from embryonic stem cells. *Cell Stem Cell* **10**, 398-411.

Malpel, S., Mendelsohn, C. and Cardoso, W. V. (2000). Regulation of retinoic acid signaling during lung morphogenesis. *Development* **127**, 3057-3067.

McCauley, K. B., Hawkins, F., Serra, M., Thomas, D. C., Jacob, A. and Kotton, D. N. (2017). Efficient derivation of functional human airway epithelium from pluripotent stem cells via temporal regulation of Wnt signaling. *Cell Stem Cell* **20**, 844-857 e846.

Mori, M., Mahoney, J. E., Stupnikov, M. R., Paez-Cortez, J. R., Szymaniak, A. D., Varelas, X., Herrick, D. B., Schwob, J., Zhang, H. and Cardoso, W. V. (2015). Notch3-Jagged signaling controls the pool of undifferentiated airway progenitors. *Development* **142**, 258-267.

Mou, H., Zhao, R., Sherwood, R., Ahfeldt, T., Lapey, A., Wain, J., Sicilian, L., Izvolsky, K., Musunuru, K., Cowan, C. et al. (2012). Generation of multipotent lung and airway progenitors from mouse ESCs and patient-specific cystic fibrosis iPSCs. *Cell Stem Cell* **10**, 385-397.

Mou, H., Vinarsky, V., Tata, P. R., Brazauskas, K., Choi, S. H., Crooke, A. K., Zhang, B., Solomon, G. M., Turner, B., Bihler, H. et al. (2016). Dual SMAD signaling inhibition enables long-term expansion of diverse epithelial basal cells. *Cell Stem Cell* **19**, 217-231.

Mucenski, M. L., Wert, S. E., Nation, J. M., Loudy, D. E., Huelsken, J., Birchmeier, W., Morrisey, E. E. and Whitsett, J. A. (2003). beta-Catenin is required for specification of proximal/distal cell fate during lung morphogenesis. *J. Biol. Chem.* **278**, 40231-40238.

Mucenski, M. L., Nation, J. M., Thitoff, A. R., Besnard, V., Xu, Y., Wert, S. E., Harada, N., Taketo, M. M., Stahlman, M. T. and Whitsett, J. A. (2005). Beta-catenin regulates differentiation of respiratory epithelial cells in vivo. *Am. J. Physiol. Lung Cell. Mol. Physiol.* **289**, L971-L979.

Nabhan, A., Brownfield, D. G., Harbury, P. B., Krasnow, M. A. and Desai, T. J. (2018). Single-cell Wnt signaling niches maintain stemness of alveolar type 2 cells. *Science* **359**, 1118-1123.

Nikolic, M. Z., Caritg, O., Jeng, Q., Johnson, J. A., Sun, D., Howell, K. J., Brady, J. L., Laresgoiti, U., Allen, G., Butler, R. et al. (2017). Human embryonic lung epithelial tips are multipotent progenitors that can be expanded in vitro as long-term self-renewing organoids. *eLife* **6**, e26575.

Ostrin, E. J., Little, D. R., Gerner-Mauro, K. N., Sumner, E. A., Rios-Corzo, R., Ambrosio, E., Holt, S. E., Forcioli-Conti, N., Akiyama, H., Hanash, S. M. et al. (2018). beta-Catenin maintains lung epithelial progenitors after lung specification. *Development* **145**, dev160788.

Patel, P. and Woodgett, J. R. (2017). Glycogen synthase kinase 3: a kinase for all pathways? *Curr. Top. Dev. Biol.* **123**, 277-302.

Que, J., Okubo, T., Goldenring, J. R., Nam, K.-T., Kurotani, R., Morrisey, E. E., Taranova, O., Pevny, L. H. and Hogan, B. L. (2007). Multiple dose-dependent roles for Sox2 in the patterning and differentiation of anterior foregut endoderm. *Development* **134**, 2521-2531.

Roccio, M., Schmitter, D., Knobloch, M., Okawa, Y., Sage, D. and Lutolf, M. P. (2013). Predicting stem cell fate changes by differential cell cycle progression patterns. *Development* **140**, 459-470.

Rock, J. R., Onaitis, M. W., Rawlins, E. L., Lu, Y., Clark, C. P., Xue, Y., Randell, S. H. and Hogan, B. L. (2009). Basal cells as stem cells of the mouse trachea and human airway epithelium. *Proc. Natl. Acad. Sci. USA* **106**, 12771-12775.

Rock, J. R., Gao, X., Xue, Y., Randell, S. H., Kong, Y. Y. and Hogan, B. L. (2011). Notch-dependent differentiation of adult airway basal stem cells. *Cell Stem Cell* **8**, 639-648.

Rockich, B. E., Hrycaj, S. M., Shih, H. P., Nagy, M. S., Ferguson, M. A., Kopp, J. L., Sander, M., Wellik, D. M. and Spence, J. R. (2013). Sox9 plays multiple

roles in the lung epithelium during branching morphogenesis. *Proc. Natl. Acad. Sci. USA* **110**, E4456-E4464.

Roost, M. S., van Iperen, L., Ariyurek, Y., Buermans, H. P., Arindrarto, W., Devalla, H. D., Passier, R., Mummery, C. L., Carlotti, F., de Koning, E. J. et al. (2015). KeyGenes, a tool to probe tissue differentiation using a human fetal transcriptional atlas. *Stem Cell Reports* **4**, 1112-1124.

Shu, W., Guttentag, S., Wang, Z., Andl, T., Ballard, P., Lu, M. M., Piccolo, S., Birchmeier, W., Whitsett, J. A., Millar, S. E. et al. (2005). Wnt/beta-catenin signaling acts upstream of N-myc, BMP4, and FGF signaling to regulate proximal-distal patterning in the lung. *Dev. Biol.* **283**, 226-239.

Swarr, D. T. and Morrisey, E. E. (2015). Lung endoderm morphogenesis: gasping for form and function. *Annu. Rev. Cell Dev. Biol.* **31**, 553-573.

Treutlein, B., Brownfield, D. G., Wu, A. R., Neff, N. F., Mantalas, G. L., Espinoza, F. H., Desai, T. J., Krasnow, M. A. and Quake, S. R. (2014). Reconstructing lineage hierarchies of the distal lung epithelium using single-cell RNA-seq. *Nature* **509**, 371-375.

Tsao, P.-N., Chen, F., Izvolsky, K. I., Walker, J., Kukuruzinska, M. A., Lu, J. and Cardoso, W. V. (2008). Gamma-secretase activation of notch signaling regulates the balance of proximal and distal fates in progenitor cells of the developing lung. *J. Biol. Chem.* **283**, 29532-29544.

Tsao, P.-N., Vasconcelos, M., Izvolsky, K. I., Qian, J., Lu, J. and Cardoso, W. V. (2009). Notch signaling controls the balance of ciliated and secretory cell fates in developing airways. *Development* **136**, 2297-2307.

Weaver, M., Dunn, N. R. and Hogan, B. L. (2000). Bmp4 and Fgf10 play opposing roles during lung bud morphogenesis. *Development* **127**, 2695-2704.

Weaver, T. E., Na, C.-L. and Stahlman, M. (2002). Biogenesis of lamellar bodies, lysosome-related organelles involved in storage and secretion of pulmonary surfactant. *Semin. Cell Dev. Biol.* **13**, 263-270.

Whitsett, J. A., Wert, S. E. and Weaver, T. E. (2010). Alveolar surfactant homeostasis and the pathogenesis of pulmonary disease. *Annu. Rev. Med.* **61**, 105-119.

Willert, K. and Nusse, R. (2012). Wnt proteins. *Cold Spring Harbor Perspect. Biol.* **4**, a007864.

Wong, A. P., Bear, C. E., Chin, S., Pasceri, P., Thompson, T. O., Huan, L.-J., Ratjen, F., Ellis, J. and Rossant, J. (2012). Directed differentiation of human pluripotent stem cells into mature airway epithelia expressing functional CFTRTR protein. *Nat. Biotechnol.* **30**, 876-882.

Xu, K., Nieuwenhuis, E., Cohen, B. L., Wang, W., Canty, A. J., Danska, J. S., Coultas, L., Rossant, J., Wu, M. Y. J., Piscione, T. D. et al. (2010). Lunatic Fringe-mediated Notch signaling is required for lung alveogenesis. *Am. J. Physiol. Lung Cell. Mol. Physiol.* **298**, L45-L56.

Xu, K., Moghal, N. and Egan, S. E. (2012). Notch signaling in lung development and disease. *Adv. Exp. Med. Biol.* **727**, 89-98.

Yamamoto, Y., Gotoh, S., Korogi, Y., Seki, M., Konishi, S., Ikeo, S., Sone, N., Nagasaki, T., Matsumoto, H., Muro, S. et al. (2017). Long-term expansion of alveolar stem cells derived from human iPS cells in organoids. *Nat. Methods* **14**, 1097-1106.

Yang, J., Hernandez, B. J., Martinez Alanis, D., Narvaez del Pilar, O., Vila-Ellis, L., Akiyama, H., Evans, S. E., Ostrin, E. J. and Chen, J. (2016). The development and plasticity of alveolar type 1 cells. *Development* **143**, 54-65.

Yang, Y., Riccio, P., Schotsaert, M., Mori, M., Lu, J., Lee, D. K., Garcia-Sastre, A., Xu, J. and Cardoso, W. V. (2018). Spatial-temporal lineage restrictions of embryonic p63(+) progenitors establish distinct stem cell pools in adult airways. *Dev. Cell* **44**, 752-761 e754.

Yugawa, T., Nishino, K., Ohno, S., Nakahara, T., Fujita, M., Goshima, N., Umezawa, A. and Kiyono, T. (2013). Noncanonical NOTCH signaling limits self-renewal of human epithelial and induced pluripotent stem cells through ROCK activation. *Mol. Cell. Biol.* **33**, 4434-4447.

Zacharias, W. J., Frank, D. B., Zepp, J. A., Morley, M. P., Alkhaleel, F. A., Kong, J., Zhou, S., Cantu, E. and Morrisey, E. E. (2018). Regeneration of the lung alveolus by an evolutionarily conserved epithelial progenitor. *Nature* **555**, 251-255.

Zhang, Y., Goss, A. M., Cohen, E. D., Kadzik, R., Lepore, J. J., Muthukumaraswamy, K., Yang, J., DeMayo, F. J., Whitsett, J. A., Parmacek, M. S. et al. (2008). A Gata6-Wnt pathway required for epithelial stem cell development and airway regeneration. *Nat. Genet.* **40**, 862-870.